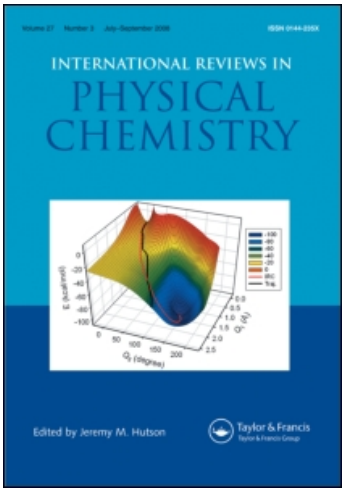

International Reviews in Physical Chemistry
Publication details, including instructions for authors and subscription information:
http://www.informaworld.com/smpp/title~content=t713724383

High resolution Fourier transform spectroscopy of jet-cooled molecules

Michel Herman; Robert Georges; Martin Hepp; Daniel Hurtmans

Online publication date: 26 November 2010

To cite this Article Herman, Michel , Georges, Robert , Hepp, Martin and Hurtmans, Daniel(2000) 'High resolution Fourier transform spectroscopy of jet-cooled molecules', International Reviews in Physical Chemistry, 19: 2, 277 — 325
To link to this Article: DOI: 10.1080/01442350050020905
URL: http://dx.doi.org/10.1080/01442350050020905

INT. REVIEWS IN PHYSICAL CHEMISTRY, 2000, VOL. 19, NO. 2, 277–325

High resolution Fourier transform spectroscopy of jet-cooled molecules

MICHEL HERMAN†*, ROBERT GEORGES‡,
MARTIN HEPP§¶ and DANIEL HURTMANS†‖
† Laboratoire de Chimie Physique Moléculaire CPi160/09,
Université Libre de Bruxelles, Av. F. D. Roosevelt, 50, B-1050 Bruxelles, Belgium
‡ Laboratoire PALMS, UMR 6627 CNRS, Université de Rennes I,
Campus de Beaulieu, F-35042 Rennes, France
§ I. Physikalisches Institut, Universität zu Köln, Zülpicher Str. 77,
D-50937 Köln, Germany

The spectroscopic literature reporting on the coupling between Fourier transform spectrometers and supersonic jet expansions is reviewed. Particular attention is devoted to high resolution infrared absorption experiments. Short and much longer introductions are provided on Fourier transform spectrometers and jets, respectively, with emphasis on the problems raised by coupling the two techniques. Details of the optical designs reported in the literature are considered. The literature on all the molecules studied is tabulated. Some of the spectroscopic results are highlighted, in particular those obtained at Université Libre de Bruxelles.

Contents

* E-mail: mherman@ulb.ac.be
¶ Present address: Bayer AG, Informatics IM-KSB TKB, Geb. B 151, D-51368 Leverkusen, Germany.
‖ Senior Research Assistant with the Fonds National de la Recherche Scientifique, Belgium.

International Reviews in Physical Chemistry ISSN 0144-235X print/ISSN 1366-591X online
http://www.tandf.co.uk/journals

1. Introduction

Levy and co-workers pioneered the implementation of supersonic jet expansions in the field of high resolution spectroscopy in the 1970s [1, 2]. In supersonic jets, gases are expanded from a higher to a lower pressure chamber through a suitable small orifice. This can be a pinhole, a confining flow nozzle, a slit or a multinozzle assembly. The free mean path in the gas and the orifice dimensions are such that a large number of collisions take place at the initial stage of the expansion. As a result a flow of molecules is produced, moving in one direction at supersonic speed and in a collision-free regime. The resulting drastic decrease of the rotational temperature leads to a spectacular spectral simplification, allowing the spectrum of larger molecules to be reliably investigated. Because the molecular speeds become aligned, spectroscopic sub-Doppler resolution conditions can be obtained without the use of high power saturating lasers. In addition, molecular complexes and clusters are being built-up by long range interaction forces in the initial phase of the jet formation, and remain longer in the expansion, hence favouring their spectral investigation. Thus, because of *spectral simplification, sub-Doppler resolution and formation of complexes and aggregates*, supersonic jet expansions opened up a new era in the characterization of intramolecular and intermolecular properties within the field of high resolution spectroscopy. Supersonic jets are today a central feature in a variety of studies in physical chemistry. It is interesting to note that a number of studies of jet-cooled molecules are reported in the literature that are based on microwave spectrometers, a very active field (e.g. [3, 4]), and also on ultraviolet spectrographs (e.g. [5–8]), in addition to laser and Fourier transform spectrometer-based experiments, as reported below.

Fourier transform spectrometers (FTS) started invading the field of high-resolution spectroscopy at about the same period supersonic jets did, that is some twenty years ago when commercial instruments became available. FTS very quickly replaced conventional monochromators and spectrographs in most spectral ranges because of the numerous advantages they provide. The multiplex recording, the broadband coverage, the calibration facilities and the computer control indeed proved to be decisive in the competition with grating-based, slit instruments. FTS today even access the vacuum ultraviolet region despite the very severe optical conditions required at such short wavelength spectral ranges to achieve high resolution Michelson interferometry.

The first report of an instrumental combination of FTS and supersonic expansions was in 1981, by Snavely *et al.* from Yale University [9]. In the infrared range, the competition between FTS and lasers is obviously very strong since both types of instrument access identical spectral regions. Laser sources appear to be ideally suited to probe supersonic expansions (see [10–12] among numerous references for infrared laser work). They indeed provide reduced instrumental linewidth, adapted to sub-Doppler investigation. They also lead to optimized sensitivity through a variety of instrumental techniques, allowing species in low concentration to be observed in the expansion. In addition, laser beams can be precisely directed, allowing a defined spatial region in the expansion, corresponding to precise experimental conditions, to be probed. FTS unfortunately fail to provide similar characteristics and, initially, one could have doubted the interest of investigating jet-cooled molecules using FTS in spectral ranges in which laser sources were also available.

Today, however, some twenty years after supersonic jets and FTS separately started their career in high resolution spectroscopy, a prolific research area has

settled around their combined use. Altogether, we spotted over 100 papers in the international refereed literature published up to the fall of 1999, which are based on the use of FTS to investigate supersonically jet-cooled molecules. A complete overview of Fourier transform (FT) FT–jet spectroscopy demonstrates that a variety of experiments were performed, including infrared absorption and emission techniques as well as the study of electronic transitions in emission. All these papers will be mentioned but the focus of the present review is set on *high resolution* and *absorption* FT–jet spectroscopy to probe *vibration–rotation spectra*. In this specific field, following the first experiment already mentioned and corresponding to medium resolution conditions, Quack and his group at Eidgenössische Technishe Hochschule (ETH) Zürich reported in 1984 Fourier transform infrared (FTIR) spectra of jet-cooled molecules at high spectral resolution [13]. This group has since been very productive in this area. In addition to a number of more isolated studies, such as those from Barnes and Gough [14] in 1987, and from Winnewisser *et al.* at Giessen, initiated in 1991 [15], four other research groups started investing more systematically in this field. They are listed below in order of their first publication on the subject: Université Libre de Bruxelles (ULB) Belgium [16], Texas A&M-USA [17], Monash-Australia [18], and Paris VI-France [19]. Additional groups are now working along similar lines, such as those from Rennes (France) [20], Göttingen (Germany) [21, 22] and Orsay (France) [23].

As an introductory illustration of FT–jet achievements, figures 1 and 2 present results of the investigation of the infrared spectrum of N_2O_4 achieved at ULB. Dinitrogen hemitetroxide is in chemical equilibrium with its monomer, NO_2, and both species are therefore simultaneously observed in the FTIR absorption spectrum recorded in a cell, as presented in figure 1 (*a*). Temperature conditions slightly lower than room temperature were used to record the cell spectrum in figure 1 (*a*) ($T = -50°C$), to raise the relative amount of the dimer. As exemplified on the spectrum in figure 1 (*b*), the spectral congestion in each of the bands of N_2O_4 on the cell spectrum prevents detailed investigation from being achieved. The spectra at the bottom of figure 1 (parts (*c*) and (*d*)) demonstrate that FT spectroscopy in supersonic jet expansions provides the required simplification and allows the rotational structure to be unravelled in N_2O_4. Those recent spectra, from [26], extend and improve previous FT-based investigations of this molecule [27–29]. One should notice that the resolution (0.005 cm^{-1} apodized resolution) and the signal-to-noise ratio (close to 100 for the strongest line) are not as good as those achieved in a diode laser investigation also reported in the literature [30]. The latter study, however, could only cover very limited parts of the full range in figure 1 due to the characteristics of the diode laser used. It did, among other drawbacks, not spot the bands presented in figure 2.

It is the purpose of sections 2 and 3 to detail the instrumental features behind FTS in connection with the investigation of supersonic expansions. A short introduction on FTS is given in section 2. This section also provides a much more solid introduction to supersonic expansions, to help understand the specificity of the various optical designs built to adapt FTS to supersonic expansions, which are detailed in section 3. Section 3 also highlights the basics of all relevant types of nozzles. Section 4 reviews the FT–jet literature, listing all papers, thus including emission work and the study of electronic transitions. Section 4 details some of the results in the field of high resolution infrared absorption spectroscopy, in particular those achieved at ULB.

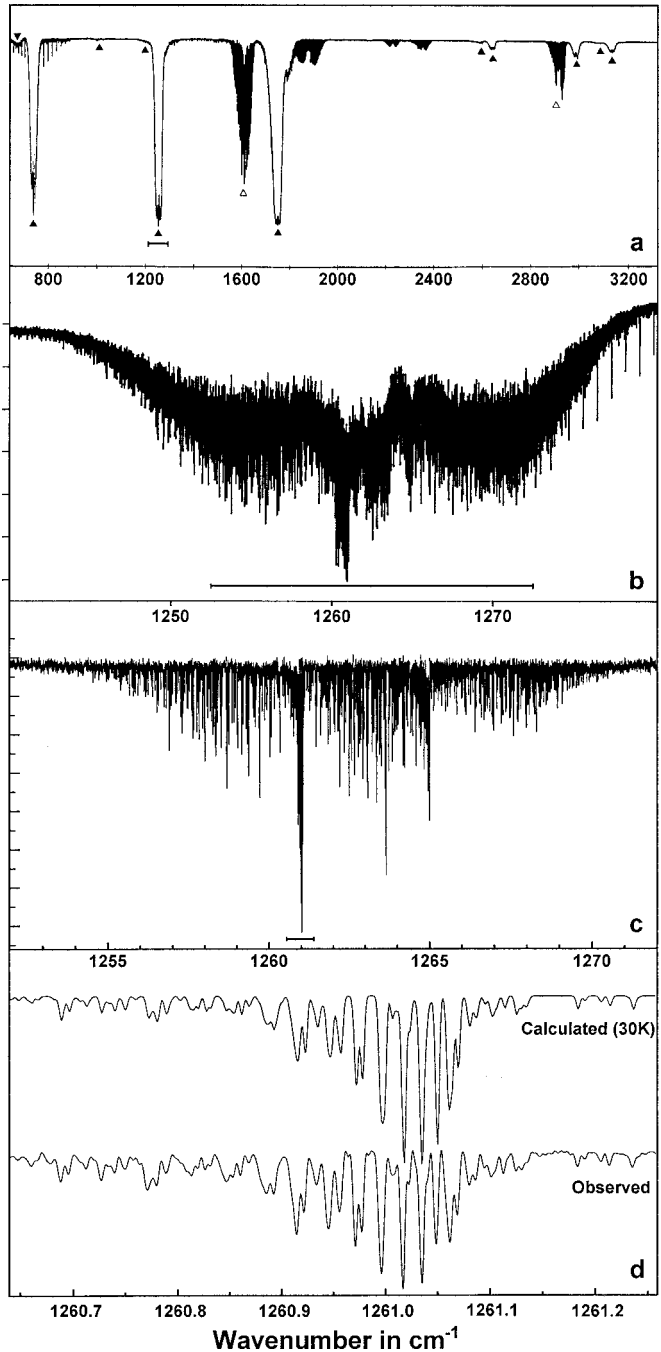

Figure 1. Infrared transmittance spectrum of N_2O_4 recorded using a FT spectrometer (adapted from [24–26], ULB data); (*a*) low resolution spectrum under −50°C temperature conditions showing absorption by NO_2 (△) and N_2O_4 (▲) simultaneously present in the sample because of the chemical equilibrium connecting the monomer and dimer species; (*b*) band centred at 1260 cm^{-1} recorded under room temperature conditions; (*c*) same band recorded under jet-cooled conditions (1:1 mixture of Ar:NO_2/N_2O_4, 40 scans, 0.005 cm^{-1} resolution, T_{rot} = 30 K); (*d*) portion of the recording in (*c*) with a comparison with the simulated spectrum.

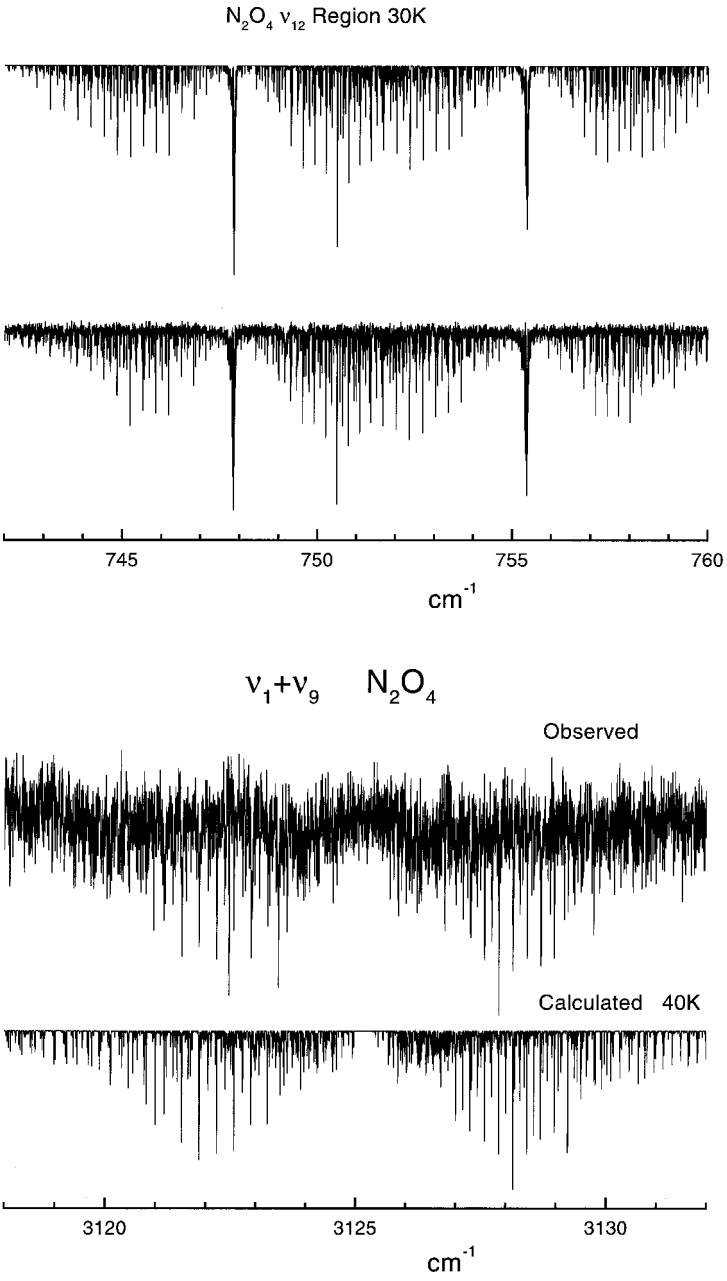

Figure 2. Infrared transmittance spectrum of N_2O_4 recorded under jet-cooled conditions using a FT spectrometer (adapted from [26], ULB data); top: bands centred around 750 cm^{-1} (4:3 mixture of Ar:NO_2/N_2O_4, 40 scans, 0.005 cm^{-1} resolution, T_{rot} = 30 K) with a comparison with the simulated spectrum; bottom: band centred around 3125 cm^{-1} (10:7 mixture of Ar:NO_2/N_2O_4, 200 scans, 0.005 cm^{-1} resolution, T_{rot} = 40 K) with a comparison with the simulated spectrum.

2. Basics of Fourier transform spectrometers and supersonic expansions

2.1. *Fourier transform spectrometers*

Fourier transform spectroscopy was first introduced in 1895 by Michelson [31] who probably measured the very first FT spectrum. Since then the technique has become quite evolved and microcomputers have helped in the production of affordable commercial equipment since the early 1980s. Users interested in basic developments are referred to various textbooks [32, 33] concerned with Fourier transform spectroscopy and its applications, and to early references [34–41]. We focus hereafter on features more relevant to FT–jet spectroscopy.

Basically, FTS uses the interference pattern produced by a two-arm Michelson interferometer. One of the mirrors is moving along one of the arms and a variable optical path difference is produced between the two sides of the interferometer. The resulting interference pattern is given by:

$$I(x) = \frac{1}{2}\int_0^\infty B(\tilde{\nu})(1 + \cos(2\pi\tilde{\nu}x))\,\mathrm{d}\tilde{\nu}, \tag{1}$$

with x the optical path difference between the two arms, $B(\tilde{\nu})$ the spectrum of the light source and $\tilde{\nu}$ the wavenumber. The oscillating part of equation (1) is recorded at equally spaced values of x, defining the 'interferogram', which samples discretely the cosine Fourier transform of the spectrum of the light source. The corresponding spectrum is then retrieved by inverting the FT using a digital fast Fourier transform algorithm [42, 43].

Among the well-known advantages of FTS versus dispersive techniques, one should highlight the combination of a number of features: (i) the digital treatment of the signal, (ii) the multiplex (or Felgett) advantage, meaning that each point of the interferogram contains information about the whole spectrum and that the noise is distributed along the whole recorded range thus increasing the signal-to-noise ratio, and (iii) the 'all the spectrum at once' benefit, which means that a spectrum over a broad spectral range can be recorded in a single experiment, at high spectral resolution.

Since the interferogram can only be recorded over a finite path difference, L (usually a few metres), a truncation occurs which limits the spectral resolution. Usually the resolution is defined as $0.5/L$, for example for interferometers built by the Bomem company, but one finds some other more conservative definitions like $0.9/L$ used, for instance, for the instruments built by the Bruker company.

As far as FT–jet spectroscopy is concerned, one of the most limiting factors is the time required to record a spectrum. Optimal resolution with commercial instruments, as for example available with the Bruker IFS120HR spectrometer used at ULB, is of the order of 1.86×10^{-3} cm^{-1}. It corresponds to a maximum optical path difference of 483 cm. Since in typical working conditions the mirror moves at a speed of about 1.25 cm s^{-1}, that is an optical velocity of 2.5 cm s^{-1}, the time required to scan a single 'full resolution' interferogram is of about 3 min. To increase the signal-to-noise ratio, an accumulation of more than 100 scans is not uncommon. The signal-to-noise ratio indeed increases as the square root of the number of co-added scans. Thus, under such conditions, the total acquisition time climbs to about 5 h. This means that the expansion has to be fed with huge quantities of gas. As an example, the spectrum of figure 3, which was obtained at the optimal resolution available at ULB (1.86×10^{-3} cm^{-1}) and which will be referred to again later in the text, corresponds to 40 min recording time, which accumulates only 12 scans. The gas consumption

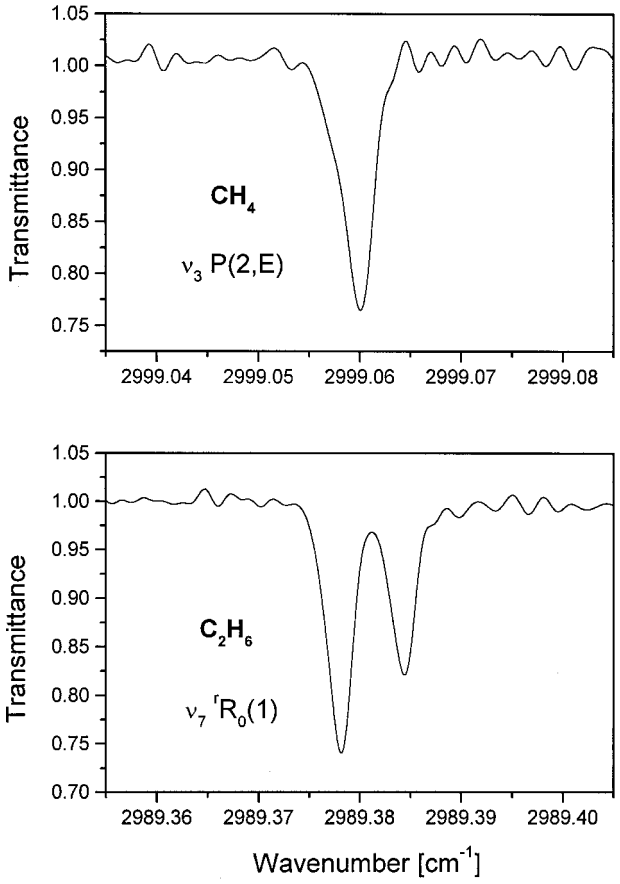

Figure 3. Very high resolution (0.001 86 cm^{-1} instrumental resolution) transmittance slit-jet-cooled spectra (boxcar apodization, 12 scans co-added, 97.5:2.5 mixture of Ar:Gas) of CH_4 and of C_2H_6. The measured linewidths on the spectra (FWHM) are 0.0034 and 0.0030 cm^{-1}, respectively, i.e. about twice the instrumental linewidth but about one third of the Doppler width at room temperature for methane. The excess width on the spectrum is partly attributed to the residual Doppler effect at the ends of the slit sections (adapted from [44], ULB data).

for the existing flow conditions for the ULB slit-jet (20 L min^{-1} continuous flow, $p_0 \approx 20$ kPa) is of about 800 L. High spectral resolution is thus achieved at the expense of gas consumption. This explains why somewhat lower resolution is usually reported in the literature. A typical value of 1×10^{-2} cm^{-1} appeared to be a good compromise in most of the ULB studies. Such a limitation is obviously much less stringent with other set-ups used in the various laboratories cited in section 4, which use pinhole expansions with, therefore, reduced amounts of gas. It should also be noted that tunable laser based investigations, usually providing higher resolution and improved sensitivity but covering much narrower spectral ranges, may also face similar problems. In other words, calculating the gas consumption in the jet per absorption line recorded could be favourable to FT-based experiments.

In conventional absorption spectroscopy, the optimal signal-to-noise ratio is achieved by increasing either the absorption path length (l), or the sample density

(n), which is proportional to the pressure (p), or even both of these parameters. In jet-cooled spectroscopy, most experimental conditions are determined by the characteristics of the expansion, many being related to the size of the nozzle, as detailed later in this review. Typically, the available absorption path is of the order of a few millimetres for a pinhole to about 20 cm for slits, while in static experiments the total absorption length can be over 100 m. Furthermore, the typical sample density remains of the order of about 10^{14} to 10^{16} cm^{-3}, while in static experiments this number can be 10^{18} to 10^{19} cm^{-3}. The reduction in the line density, leading to a concentration of the same band intensity in fewer vibration–rotation lines, does not fully compensate for these drawbacks. Therefore, high resolution FT–jet absorption spectroscopy has so far focused mainly on stronger fundamental and related hot bands in the infrared range. However, despite the anticipated lack of sensitivity and resolution achieved with FTS compared with laser-based investigations, molecular complexes, as well as weaker near-infrared bands of stable species, could be observed and analysed (see section 4). Actually, some authors claim in a convincing way [22, 45] that in specific cases, in particular whenever very high resolution is not required, FT–jet experiments prove to be highly sensitive, possibly even more than cavity ring down-laser experiments [46, 47] for the study of larger clusters at medium spectral resolution [22].

The designs developed in FT–jet spectroscopy account for the severe optical limitations of the instrument. Indeed, the absorption light beam is far from being a point and so probes the molecular beam over a wide spatial region, usually including the surrounding hotter gas. The resulting absorption thus simultaneously accounts for various, sometimes very different temperature, molecular speed and concentration conditions. The research groups involved in FT–jet spectroscopy have different responses to these constraints. The resulting designs are briefly reviewed later. We shall, in particular, highlight in section 3 those set-ups which increase the absorption path in the beam, either through multi-pass optics or using slit jets, all requiring minimization of the waist of the optical beam.

As another general comment, one should mention the problems raised by the mechanical noise created by the ever more powerful pumping units reported in the literature, further detailed in section 2.2. An important 'dead' space is usually required to set the jet assembly away from the spectrometer, necessitating the building of solid and adequate optical designs from the absorption source to the spectrometer, through to the supersonic expansion chamber. Different ways of constructing such systems are presented later.

2.2. *Supersonic expansions*

A typical evolution of a condensing gas in a supersonic expansion is presented in figure 4 (adapted from [48]). In this schematic diagram ($\ln(p), \ln(T)$), the gas starting from reservoir conditions (point A on figure 4, defining p_0 and T_0) expands along an adiabatic and reversible path (isentrope). After reaching point B on figure 4, the gas behaviour follows the isentrope in the supersaturated region up to point C determining the onset conditions for clustering. If the onset point is passed, the gas starts condensing and reaches the liquid–gas equilibrium curve. This incursion in the supersaturated region is of primary importance to study both isolated 'super-cooled' molecules and small complexes in the gas phase. Translational temperatures reached in supersonic gas expansions, corresponding to the velocity distribution, range typically from a few Kelvins to a few tens of Kelvin. Campargue even reports

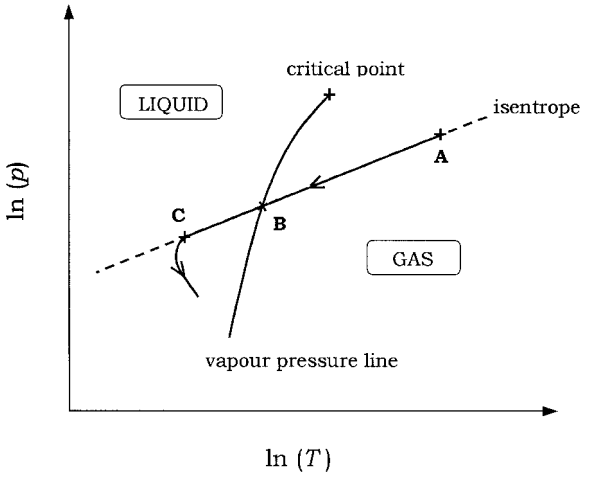

Figure 4. Schematic thermodynamic diagram (ln p, ln T) showing the evolution of a condensing gas during isentropic expansion (adapted from [48]).

a translational temperature of 6 mK obtained in a supersonic jet of helium [49]. Even at such extreme temperatures, the medium (helium in the example just mentioned) remains gaseous in the expansion, being thus highly super-saturated. This is a really significant advantage compared to static gas cells in which the gas temperature is lowered with the help of standard cryogenic techniques using refrigerating fluids (e.g. [50]). In the latter case, for a given temperature, the pressure of the gas has to be maintained under its vapour pressure $p_v(T)$ to prevent liquefaction, thus strongly limiting the amount of gaseous material and, hence, the absorption intensity. Collisional cooling techniques [51], not considered further in the present review, provide an interesting alternative way to achieve low temperatures, however they also strongly limit the amount of absorbing gaseous material.

Supersonic cooling is based upon the thermodynamic properties of the isentropic expansion of a fluid, which always leads to cooling the fluid. Practically, an isentropic expansion is realized by expanding a gas through an orifice from a stagnation reservoir at 'high' pressure p_0 (typically 100 kPa or more) into an evacuated chamber where a lower residual pressure p_r remains (typically a few hPa or less). The shape and the dimension of the orifice—or nozzle—determine both the thermodynamic and the kinetic properties of the downstream expansion. Many different nozzle geometries are reported in the literature: axisymmetric (pinholes, capillaries, converging–diverging nozzles) or planar (slit nozzle, bi-dimensional converging–diverging nozzles). They are detailed in this section and in section 3.

Two case studies are to be distinguished, depending on the relative sizes of the nozzle dimension d^* (pinhole diameter or slit width) and of the mean free path λ_0 of the molecules under stagnation conditions. One defines the nozzle Knudsen number $K_{n_0} = \lambda_0 / d^*$, which can be interpreted as a *rarefaction parameter*, i.e. K_{n_0} increases as the number of collisions experienced by a molecule decreases. When d^* is smaller than λ_0, i.e. $K_{n_0} \gg 1$, the number of collisions approaches zero when molecules leave the reservoir and, under such conditions, the velocity distribution in the reservoir is kept unchanged beyond the gas exhaust. Such an effusive molecular beam does not lead to cooling effects. In the opposite case, i.e. d^* is larger than λ_0 and $K_{n_0} \ll 1$, a

large number of collisions take place, at least during the first stage of the expansion, tending to establish an equilibrium among the gas particles. Newtonian mechanics can be applied to model the expansion and, at high reservoir pressures, the effects of gas viscosity and heat transfers on the flow are minor. It is then convenient to treat the flow as inviscid and isentropic.

The following describes the physical properties of such an adiabatic flow. For a flowing fluid the basic thermodynamic quantity is the enthalpy h (per unit mass), rather than the internal energy. These two quantities differ from each other by the 'flow work', i.e. the work due to the pressure forces moving the considered fluid volume along the flow direction. The adiabatic energy equation for unit mass is:

$$h + \tfrac{1}{2}u^2 = \text{constant}. \tag{2}$$

The second term on the left of equation (2) is the kinetic energy per unit mass. Equation (2) may be applied to the reservoir particles for which the flow velocity u in the fluid centre of mass is zero. Thus, one can write $h_0 = \text{constant}$, where h_0 denotes the stagnation or reservoir enthalpy. For a perfect gas, $h = c_p T$ and the energy equation becomes:

$$c_p T + \tfrac{1}{2}u^2 = c_p T_0. \tag{3}$$

Equation (3) shows that the available thermal energy in the reservoir at temperature T_0 is to be partially converted into kinetic energy of directed mass flow as the gas expands into the vacuum chamber. The fluid acceleration is then accompanied by a decrease in the temperature, T, of the flow. Ideally, this process stops when all the available stagnation enthalpy has been converted into kinetic energy, i.e. when the maximum flow speed $u_{\max}$ has been reached. Letting $T \to 0$ in equation (3) leads to:

$$u_{\max} = (2c_p T_0)^{1/2} = \left[\frac{2kT_0}{m_p}\left(\frac{\gamma}{\gamma - 1}\right)\right]^{1/2} \tag{4}$$

with γ the ratio of heat capacities of the gas (or Poisson coefficient), m_p the gas particle mass and k the Boltzmann constant. Equation (4) gives 1765 m s^{-1} and 558 m s^{-1} for helium and argon, respectively, expanding from a reservoir at $T_0 = 300$ K. Note also that for a given mass, an increase in γ produces a decrease in the flow velocity ($u_{\max}(\gamma = 9/7) > u_{\max}(\gamma = 7/5) > u_{\max}(\gamma = 5/3)$).

The decrease of the local temperature of the flow, T, produces both a narrowing of the velocity distribution of the gas and a decrease of the most probable local thermal velocity, $u_p = (2kT/m_p)^{1/2}$. An 'observer' moving within the gas along the jet axis would notice a progressive reduction of the thermal motion of the molecules around him until they become completely still in the moving reference axis system, when the ultimate flow velocity is reached ($u \to u_{\max}$, $T \to 0$). This ideal limiting case corresponds to a cloud of 'frozen' molecules whose ensemble velocity distribution is close to a Dirac distribution located at $u_{\max}$.

In practice, a small fraction of the gas of interest is seeded into a monoatomic gas for which the cooling effect is larger, because the Poisson coefficient γ (5/3) is the largest possible (see next section). All kinds of rare gases can be used as carrier gas. Helium and argon are generally preferred because of cost considerations. In the case of a mixture of two gases, two velocities have to be considered. The interesting point is that the seeded gas reaches the final temperature of the carrier gas. For more

detailed information on the subject, see the 'Pocket Model of Seeded Supersonic Beams' by DePaul *et al*. [52].

One accesses the thermodynamic properties of the expanding flow using equation (2). The prediction of the local translational temperature $T(\delta)$, local pressure $p(\delta)$, local density $\rho(\delta) = 1/v(\delta)$, with v the volume of a unit mass of gas, and local molecular number density $n(\delta)$, expressed in terms of the dimensionless distance $\delta = x/d^*$, that is the distance from the nozzle in diameter units, requires the additional knowledge of the evolution of the flow velocity, $u(\delta)$. In a compressible fluid, the flow velocity and the flow density are linked in a non-trivial way by the one-dimensional continuity equation (law of conservation of mass), using the mass flow rate ($\dot{m}$):

$$\dot{m} = \rho u A = \text{constant}, \tag{5}$$

where A is the cross-sectional area of the stream tube considered. Moreover, in compressible flow theory the pressure–density relation for the fluid plays a central role. This relation naturally introduces the speed of sound a:

$$a^2 = \left(\frac{\partial p}{\partial \rho}\right)_s = \frac{\gamma k T}{m_p}, \tag{6}$$

where the subscript s in this case specifies an isentropic process. In a flowing fluid, the flow speed relative to the speed of sound is a meaningful dimensionless parameter, called the Mach number (M), which measures the compressibility of the flow:

$$M(\delta) = \frac{u(\delta)}{a(\delta)}. \tag{7}$$

From equations (3), (6) and (7), one finds the temperature evolution of the expanding gas:

$$\frac{T(\delta)}{T_0} = \frac{2}{2 + (\gamma - 1)M^2(\delta)}. \tag{8}$$

Furthermore one can use the following standard isentropic relations for a perfect gas to connect to M, through equation (8), the ratios p/p_0, ρ/ρ_0 and n/n_0 (at specific δ values):

$$\frac{p}{p_0} = \left(\frac{\rho}{\rho_0}\right)^{\gamma} = \left(\frac{n}{n_0}\right)^{\gamma} = \left(\frac{T}{T_0}\right)^{\gamma/(\gamma-1)}. \tag{9}$$

Finally, equation (7) may be rewritten using equations (6) and (8) to express the flow velocity as:

$$u = M\left(\frac{\gamma k T_0}{m_p}\right)^{1/2}\left(\frac{2}{2 + (\gamma - 1)M^2}\right)^{1/2}. \tag{10}$$

In the case of seeded beams, equations (8)–(10) can be applied using the following specific-heat ratio γ_{mix} of the mixed gas:

$$\frac{1}{\gamma_{mix} - 1} = \frac{X_s}{\gamma_s - 1} + \frac{1 - X_s}{\gamma_c - 1}. \tag{11}$$

γ_s and γ_c are the specific-heat ratios of the seeded gas and the carrier gas, respectively. X_s is the mole fraction of the seeded gas.

The flow Mach number plays a central role in equations (8) to (10). This quantity only depends on the nozzle geometry and on the ratio of heat capacities of the gas or of the gas mixture. It can be determined numerically using the method

of characteristics [53]. The resulting numerical curves $M(\delta)$ can then be fitted by adjusting the free parameters of various analytical functions. Such a procedure is illustrated in section 3.

Let us now describe the different flow regimes taking place during an isentropic expansion, considering for simplicity a gas escaping from a pinhole. If the chamber pressure is kept lower than the stagnation pressure, the gas will be forced to move through the pinhole. A bundle of converging and diverging streamlines will form respectively above and below the pinhole (see figure 5). The fluid enclosed in this converging–diverging stream tube structure is subject to different flowing regimes governed by the area–velocity relation (see e.g. [55]):

$$\frac{\mathrm{d}u}{u} = \frac{-\mathrm{d}A/A}{1-M^2}. \tag{12}$$

This relation shows that sonic speed ($M = 1$) can be attained only if the section remains constant ($\mathrm{d}A/A = 0$). The flow variables corresponding to a point where conditions are sonic in the expansion will be henceforth denoted by the superscript *. According to equations (8) and (9), the sonic pressure relative to the reservoir pressure then drops to:

$$\frac{p^*}{p_0} = \left(\frac{2}{\gamma+1}\right)^{\gamma/(\gamma-1)}. \tag{13}$$

Equation (13) leads to pressure ratios of 0.487 and 0.528 for an ideal monoatomic gas ($\gamma = 5/3$) and an ideal diatomic rigid gas ($\gamma = 7/5$), respectively.

The condition $M = 1$ at the throat will only be reached provided the pressure in the residual chamber (p_r) is lower than the sonic pressure, that is if the condition $p_r < p^*(\approx p_0/2)$ is fulfilled. In this case, beyond the nozzle, the flow bifurcates towards the supersonic ($M > 1$) branch ($p_r = p^*$ corresponds to the limiting case separating subsonic and supersonic branches). Equation (12) shows that, when $M > 1$, the increase of the stream tube section area beyond the nozzle exit produces an increase in velocity. The flow below the throat is thus continuously accelerated. Such an expansion, which is unsymmetrical because two otherwise identical areas situated in the subsonic region and in the supersonic region do not correspond to the same flow velocity, is currently called a 'supersonic' expansion. The flow velocity is, however, limited to the ultimate value u_{max} and, practically, the most significant effect in the residual chamber is the decrease of the flow density (see later figure 8). As a result, high M values, up to $M = 20$ or more are obtained locally.

A supersonic expansion formed by expanding a gas through a simple orifice not containing nozzle walls is termed 'free jet', as distinct from jets arising from expansions forced through converging–diverging channels.

It is interesting to note that, for a given stagnation pressure (p_0), the amount of fluid forced through the nozzle is fixed once the sonic pressure is reached at the throat. The mass flow rate at the nozzle becomes insensitive to any further decrease in the residual pressure (p_r). The mass flow rate is then calculated using equation (5) under sonic conditions:

$$\dot{m} = \rho^* u^* A^* = p_0 A^* \left[\frac{\gamma m_p}{kT_0}\left(\frac{2}{\gamma+1}\right)^{(\gamma+1)/(\gamma-1)}\right]^{1/2} \tag{14}$$

with $A^* = \pi d^{*2}/4$ for an axisymmetric nozzle and $A^* = d^* l$ for a planar nozzle of length l.

2.3. *Relaxation processes*

Different molecular relaxation processes are connected to the two-body collisions experienced by the molecules in the jet. The total number of binary collisions during the flow expansion, for each molecule, scales as the so-called relaxation parameter $p_0 d^*$. We have assumed in the previous section that the flow follows the idealized continuum model, thus implying that the number of intermolecular collisions is large enough to equilibrate the various molecular degrees of freedom. Under such conditions, the translational ($T = T_t$), vibrational (T_{vib}) and rotational (T_{rot}) temperatures would remain identical.

The translational energy exchanges occur very rapidly so that the translational temperature T_t appearing in all equations provided so far remains properly defined. Rotational relaxation is somewhat less efficient and needs therefore, a somewhat greater number of collisions to equilibrate with translation. This number is much larger, on the order of 10^2–10^4, for a complete vibrational relaxation to occur [56]. Unfortunately, the decrease of molecular density along the flow axis induces a continuous drop in the collision frequency, so that the total number of collisions experienced by a molecule (typically of the order of 10^2 [54]) is, in general, just sufficient to permit complete rotational relaxation but not complete vibrational relaxation. This is a well known phenomenon, also considered by authors using FTS (see e.g. [57–59]). Thus one needs to define various temperatures in the jet, each related to a different molecular internal degree of freedom, with $T_{vib} > T_{rot} \geqslant T_t$ (see e.g. [60]).

At some point downstream of the gas exhaust, the number of binary collisions is not sufficient to equilibrate the translation. At this particular point, the continuum model becomes invalid, the cooling stops and the Mach number reaches a terminal value. This onset of non-equilibrium effects can be estimated by calculating the local or jet Knudsen number K_n defined as the ratio of the mean free path in the laboratory system λ to the scale length of the temperature field $l_T = T/|\mathrm{d}T/\mathrm{d}x|$ [48]:

$$K_n = \frac{\lambda}{l_T} = \frac{\lambda}{\mathrm{d}x}\left|\frac{\mathrm{d}T}{T}\right|. \tag{15}$$

For a hard sphere gas, non-equilibrium effects are assumed to become significant for the translational temperature if $K_n > 0.04$ [48].

Beyond the value of $K_n = 0.04$, the collisions are so infrequent that the distribution function of the velocity component parallel to the jet axis stops evolving, i.e. the temperature $T_{\|}$ relative to this motion is fixed. On the other hand, the dispersion of perpendicular velocities still increases since the molecules with large perpendicular components of velocity move away from the jet axis as the distance from the nozzle increases. This purely geometrical effect leads to narrowing of the perpendicular velocity distribution and hence to translational temperature decrease. Finally, beyond the terminal Mach number one reaches $T_{vib} > T_{rot} > T_{\|} > T_{\perp}$.

Various spectroscopic and fundamental insights arose in the FT spectrometer literature from the study of the different temperatures in the jet. Concerning the vibration degrees of freedom, the large amplitude motions such as, in particular, the torsion, are very efficiently cooled under free jet experimental conditions. A number of studies, concerning N_2O_4 (e.g. [26], see figure 1), C_2O_5 (see later figure 22 [61]) and $1,2C_2H_4Cl_2$ [62], among other species, indeed confirmed that the cooling of the low frequency vibrations is efficient enough to lead to a spectacular decrease

in line density in the jet-cooled spectra, allowing the rotational structure of the main vibrational bands to be analysed. Such specific vibration degrees of freedom seem thus to behave very similarly to rotation, as far as the cooling efficiency in the expansion is concerned. Other cooling effects and related temperatures were also investigated, such as spin orbit effects, in NO [59], and nuclear spin effects, in CH_4 [59]. In the latter case, Quack and co-workers [59] demonstrated that the collision-induced energy transfers occurring in the jet did not connect the various nuclear spin species in CH_4, leading to interesting relative line intensity features, as confirmed in additional experiments carried out using both diode lasers [63] and FTS [64] (see also [65, 66]).

All features so far reported concern *continuous* jet expansions. It is known that *pulsed* jets are more efficient in cooling the molecules than continuous expansions. Their use also obviously decreases gas consumption. Pulsed jets are therefore attractive. However, several technical limitations are encountered in the infrared range when coupling pulsed jets to FTS, explaining why so few experiments are reported in the literature. The main problem is the continuous displacement of the moving mirror of most interferometers which makes it really difficult to synchronize the pulsation of the jet with the acquisition rate of the FTS. The common sampling rate with FTS is of a few kHz while the duty cycle of the injection systems is of about 10 ms. An attempt to by-pass this problem has been made by Quack and co-workers [67] by recording the pulsed jet asynchronously. The hashing of the interferogram is partially washed out by the drift of the phase between the pulsing and the acquisition signals. This technique has interesting potential even though, as the authors admit, it has severe problems, such as the appearance of spatial harmonics in spectra. Quack, Suhm and co-workers also succeeded in coupling semi-synchronously pulsed jets to their continuous FT spectrometer [68, 69], by opening the jet valve simultaneously with each rapid scan, corresponding to low resolution conditions.

The optimal way to record spectra using pulsed jets is to use step-scan interferometers that stop the mirror motion at each recording point, allowing the FT spectrometer sampling and pulsed gas inlet to be properly synchronized. Low resolution commercial versions have been used for this purpose [22] (see also [70] for the coupling of cavity ring down laser spectroscopy with FT spectroscopy, in a cell) and home made high resolution constructions are available in some laboratories and were designed to work in the time-resolved mode (e.g. [71–76]). Note also that some commercial instruments are able to provide a pseudo step-scan function mode allowing time or pseudo-time resolved spectroscopy to be achieved in the present context by fully synchronizing the jet valve and the FT signal sampling. This technique has been used by the group of Leone with a modest resolution spectrometer to probe the result of pulsed laser excitations [77, 78] and also by Lindner *et al.* [79] for pulsed jet experiments combining pulsed laser excitation and low resolution recording. Zhu and co-workers used this pseudo time-resolved operation for FT-coupled ICLAS type experiments in a static cell [80, 81].

3. Details of FT–jet assemblies

3.1. *Pinhole expansions*

Initially in the literature, the first supersonic jet sources to be combined with FTS were circular nozzles. Such nozzles, made from steel, aluminium or non-conductive materials such as Pyrex or quartz if used with high voltage discharges, are still

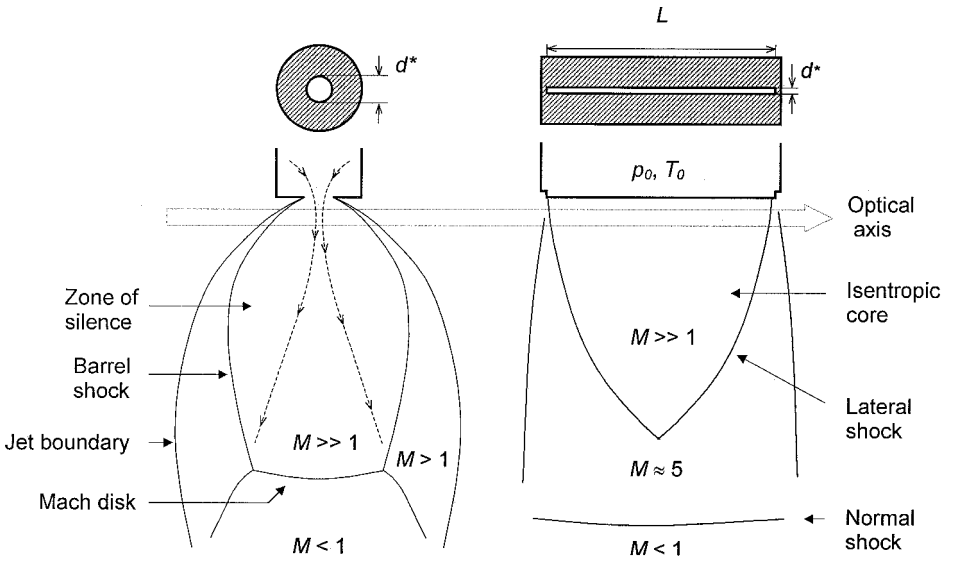

Figure 5. Flow structure of axisymmetric and planar free jets (adapted from [54]).

widely used in FT–jet experiments. Their diameters usually vary from 100 μm up to 2 mm (see table 1).

Figure 5 shows the structure of a free jet produced through a pinhole nozzle, from pictures taken using light-scattering techniques, such as Schlieren photographs. This structure includes an axisymmetric core enclosed in a system of shock waves. Shock waves are very thin regions characterized by a strong gradient of the various flow parameters. They can be seen as discontinuity regions across which the flow parameters (thermodynamic variables, velocity, Mach number and so on) are jumping between very different values in a very short distance, of the order of one local mean free path†. A shock wave is a non-isentropic process induced by the supersonic regime of the flow. As the gas travels faster than the perturbations which it generates, propagating at the local speed of sound, the supersonic gas 'ignores' the boundary conditions of the vacuum chamber in which it evolves. As a consequence, the supersonic gas overexpands to a pressure considerably lower than p_r and is abruptly recompressed by shocks [53]. For example, a supersonic flow characterized by $M_1 = 10$ just upstream of a normal shock, reaches $M_2 = 0.45$ after crossing the shock. In this example, according to equation (9), pressure, density, temperature and flow velocity ratios between upstream and downstream conditions are calculated to be 125, 3.9, 32.2 and 0.26, respectively.

The normal shock, perpendicular to the centreline of the jet is termed the Mach disc. The lateral shock surrounding the central part of the expansion forms the barrel shock. The Mach disc and the barrel shock encapsulate the gas expansion in

† In the case of low-pressure chambers (in the 10^{-3}–10^{-4} hPa range) pumped by cryopumps or diffusion pumps, the local mean free path may be very long (up to several centimetres) so that the shock waves present a diffuse structure. This kind of expansion is often called a 'Fenn' type expansion as opposed to the 'Campargue' type expansion characterized by the presence of thin and well marked shock waves owing to a higher pressure in the chamber (10^{-1}–10^{-2} hPa).

Table 1. Major characteristics of supersonic expansions under typical FT–jet experimental conditions, as reported in selected literature references (see text for the definition of the symbols).

Nozzle dimensions	p_0(kPa)	p_r(kPa)	p_0/p_r	δ_{light}	δ_M	Nozzle flow rate[a] (mol h^{-1})	References
Cryopump							
150 μm	80	0.002	40×10^6	13	4240	0.37	[83]
240/300 μm	600	< 0.1	6×10^6	1–110[b]	1640	7.1/11.1	[18, 85–88]
500/660/1000 μm	50–200	0.013–0.13	1.5×10^6–4×10^6	1–8	820–1340	10.3/17.9/41.1	[9, 84, 89, 90]
Diffusion pump							
100/150 μm	240–675	0.9–1.5	3×10^5–4.5×10^5	10–110	370–450	1.4/3.1	[13, 28, 57, 58,
5 μm × 3 mm					21 600–29 600	2.7	67, 91–99]
250 μm	101.3	0.13	7.6×10^5	8–40[c]	585	1.3	[19, 100, 101]
300 μm	50	0.1	5×10^5	7[d]	475	0.9	[15]
10 μm × 10 mm				–	32 100	1.3	
Mechanical pump							
31 × 400 μm	138–266	50–80	1500–3000	–	–	271.3	[26, 44, 62
30 μm × 160 mm				100–300[e]	350–610	334.3	64, 113–115]
100/140 μm	2026	53	38 000	–	130	4.2/8.2	[14, 111, 112]
40 μm × 750 mm					4360	15.9	
50 μm × 38 mm	217.5	13	16 300	–	2260	108.2	[17, 45, 113–115]
250 μm	405	> 50	< 30 000	–	< 115	5.2	[116–121]
30 μm × 5 mm						15.9	
700 μm	50.65	1.33	38 000	–	130	5.1	[122]
500/2000 μm	101.3/25.3	1.33/9.33	76 000/2700	8–17	185/35	5.2/1.3	[123–126]
200 μm	1620	66	24 300	15	105	13.3	[127]
200 μm	50–150	60–120	800–1250	1–18	19–25	1.2	[128]

[a] Nozzle flow rates $\dot{N}$ have been estimated from p_0 and A^* using equation (14) and $\dot{N} = \dot{m}/W$, where W is the molar mass. Argon has been chosen ($W = 40 \times 10^{-3}$ kg, $\gamma = 5/3$) to calculate $\dot{N}$.

[b] In standard configuration nozzle height is set so that the nozzle just begins to impinge on the infrared beam.

[c] A multipass optical configuration is used, $\delta = 8$ corresponds to the first light beam and $\delta = 40$ to the last beam.

[d] Case of the pinhole.

[e] Case of the slit-jet only.

the so-called 'bottle of Mach'. Because of its above-mentioned isentropic properties, the central part of the jet is the region of spectroscopic interest. This region is also termed the silence zone in recognition of the fact that the low temperature leads to very low speeds of the sound, and hence to high Mach number values (see equation (7)).

Of practical importance is the Mach disc location x_M, or δ_M in nozzle diameters, i.e. the distance at which the flow becomes subsonic [82]:

$$\delta_M = \frac{x_M}{d^*} = 0.67 \left(\frac{p_0}{p_r} \right)^{1/2}. \tag{16}$$

The Mach disc location does not depend on the gas since equation (16) contains neither the coefficient γ nor the mass. It rather depends on the efficiency of the pumping unit, that is on the ability to maintain low residual pressure in the vacuum chamber despite high reservoir pressure.

In FT–jet experiments using cryogenic-pumped (e.g. [18, 83, 84]) or diffusion-pumped systems (e.g. [15, 19, 57]), the pressure ratios obtained are of the order of magnitude 10^6 and 10^5, respectively (see table 1). Thus the corresponding Mach disc locations are 670 and 213 in nozzle dimension units, or equivalently, 13.4 cm and 4.26 cm below a standard 200 μm diameter nozzle. The zone of silence is then large enough to be probed by the intrinsically large diameter (several millimetres) of the incoherent infrared FT light beam.

More widely used in FT–jet experiments are mechanically pumped systems (e.g. [107, 111, 113, 118, 122, 123, 127, 128]) essentially based on root blowers. Supporting higher background pressures (10–100 Pa), they can be used at higher nozzle flow rates (up to several hundred of mol h^{-1}, see table 1). The counterpart is the relatively small pressure ratio they can afford, ranging between 10^3 and 10^4. A typical ratio $p_0/p_r = 1000$ gives $\delta_M = 21$. Under such conditions, selecting a 500 μm diameter nozzle restricts the probing zone to 10.5 mm below the reservoir aperture. In this case, the Mach disc location becomes a significant constraint for the design of the FT–jet optics, as further described in section 3.2.

Thermodynamic parameters along the expansion are connected to $M(\delta)$ via equations (8)–(10). The centreline Mach number is given by [53]:

$$M = (\delta)^{(\gamma-1)/j} \sum_{n=0}^{n=3} \frac{A_n}{\delta^n}, \quad \text{for } \delta > 0.5, \tag{17}$$

$$M = 1.0 + a_2\delta^2 + a_3\delta^3, \quad \text{for } 0 < \delta < 1.0, \tag{18}$$

where, in equation (17), $j = 1$ stands for an axisymmetric jet. $j = 2$ stands for planar jets considered in a later section devoted to slit jets. The various fitted constants are listed in table 2, reproduced from [53].

Equations (17) and (18) are plotted in figure 6. This figure illustrates the more efficient cooling associated with the use of a monoatomic gas. Often, laser based experiments use very dilute mixtures with less than 1% of seeded gas. FT–jet experiments, however, usually need higher mass flow rates to compensate for their lower inherent sensitivity. In practice, carrier gases are used in moderate proportion without exceeding 50%. Expansions made of pure gases are currently used in FT–jet experiments, so that γ_{mix} is then closer to the less favourable value of the Poisson

Table 2. Numerical coefficients (reproduced from [53]) useful for characterizing the Mach number versus distance downstream from the nozzle in unidimensional units, both for axisymmetric ($j = 1$) and planar ($j = 2$) jets, for different values of γ (see text for more details).

j	γ	A_0	A_1	A_2	A_3	a_2	a_3
1	5/3	3.232	−0.7563	0.3937	−0.0729	3.337	−1.541
1	7/5	3.606	−1.742	0.9226	−0.2069	3.190	−1.610
1	9/7	3.971	−2.327	1.326	−0.311	3.609	−1.950
2	5/3	3.038	−1.629	0.9587	−0.2229	2.339	−1.194
2	7/5	3.185	−2.195	1.391	−0.3436	2.261	−1.224
2	9/7	3.252	−2.473	1.616	−0.4068	2.219	−1.231

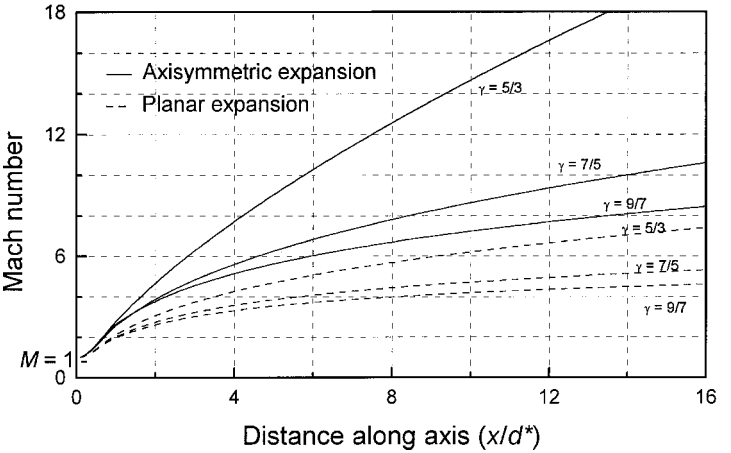

Figure 6. Mach number versus distance beyond the nozzle in one-dimensional units, for axisymmetric and planar jets and different values of γ (adapted from [53]).

coefficient of the spectroscopic gas. The resulting gain in sensitivity is then obviously connected to a loss in the cooling efficiency.

The flow, which undergoes an important part of its acceleration during the subsonic regime ($u^*/u_{max} = 0.50$; 0.41; 0.35, respectively for $\gamma = 5/3$; 7/5; 9/7), is still accelerated throughout the supersonic regime but reaches its maximum velocity very rapidly, after travelling approximately 10 nozzle diameters in the case of a monoatomic gas (see figure 7). Such a distance from the nozzle corresponds to about $M = 15$ for a monoatomic gas (see figure 6). However, as already pointed out, in practice the local Mach number increases to much higher values due to a simultaneous decrease of the flow density, which reduces the speed of sound (see equations (6) and (7)).

Inserting equation (17) into equation (9) shows that the number density n drops approximately as the square of the distance from the nozzle, as shown on figure 8. This figure also presents the evolution of other important parameters along the jet axis. This $1/\delta^2$ behaviour comes from the important spreading due to a pinhole expansion, owing to the fact that the gas is set free to expand in all directions after

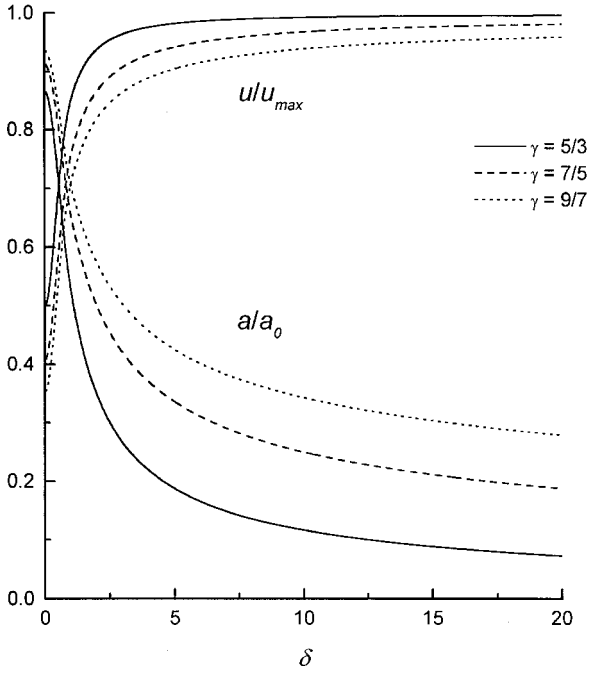

Figure 7. Relative flow velocity (u/u_{max}) and speed of sound (a/a_0) beyond a pinhole for different values of γ. An atomic gas reaches maximum flow velocity very rapidly while other gases reach this limit further away from the pinhole.

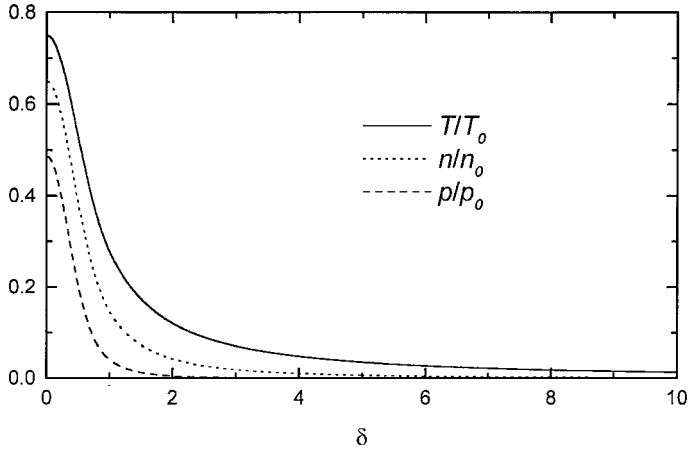

Figure 8. Evolution of the temperature, pressure and density in a pinhole expansion. The linear scale is selected to show clearly the very abrupt decrease occurring over distances corresponding to a few pinhole diameters.

escaping from the reservoir. The Doppler spread actually induces a line broadening of about 0.008 cm^{-1} (FWHM (full width at half maximum)) as measured in FT–jet experiments using a CO_2 supersonic expansion [15]. A second restriction now arises in the present circumstances. An FTIR experiment needs to maximize the number

of probed molecules in order to boost its sensitivity and it is necessary to probe the zone close to the nozzle exit, where the molecule density is highest. However, as seen in figure 8, this can only be achieved at the expense of the cooling efficiency. This figure also shows that, for FT–jet experiments, the various thermodynamic parameters in this optimal zone, located close to the nozzle, are strongly non-uniform. The rather wide FT light beam thus probes a wide range of experimental conditions. The next section highlights in the FT–jet literature some of the optics designed to deal with this specific problem. In addition, it has to be kept in mind that, depending on the value of δ, the pressure in the core expansion can be much lower than the residual chamber pressure. Therefore, unwanted absorption from background gas can arise, especially with mechanical pumps (10 Pa < p_r < 100 Pa). To mitigate this problem, which can be a significant one, the optical windows in the vacuum chamber along the FT light beam have to be placed as close as possible to the expansion. This problem is less severe when using diffusion pumps or cryopumps because of the lower background pressure, usually in the 0.001–1 Pa range.

3.2. *FT optics for pinhole expansions*

The first design reported in the FT–jet literature, by Snavely *et al.* [9, 84], involves a single pass through a pinhole jet located outside of the spectrometer. Such set-ups have to deal with the relatively large light beam issuing from the FT spectrometer. This beam is nearly parallel or converging, depending on the instrument manufacturer. The optical design must therefore be adjusted to reach a focal point at the precise position of the molecular beam.

Some authors, Quack [57, 59] and later Herman in the early ULB set-up [16] and their co-workers designed systems to work inside the spectrometer, thus exploiting the internal optical characteristics of the spectrometer provided by the manufacturer. Such set-ups face problems with the mechanical coupling between the expansion cell and the spectrometer, especially if one wishes to be able to evacuate the spectrometer, as in [57, 59]. The two parts can also be made physically completely independent, as in [16], partly compensating the vacuum problem by purging the spectrometer with dry nitrogen. In all these options, the use of a multi-pass system or a slit jet is not favoured by the reduced space available in the sample compartments fitted in commercial spectrometers.

The introduction of a double- and multi-pass system to probe expansions located outside the spectrometer was achieved by McNaughton *et al.* [18] who designed a star-shaped arrangement of the light rays, as shown in figure 9. The nearly parallel light beam of *ca.* 25 mm in diameter is reflected on 10 flat mirrors surrounding the molecular beam in such a way that the expansion is crossed 11 times. Each mirror is separately adjustable, and the region of the jet that is probed can be precisely selected. The gain in sensitivity is claimed to be about a factor of 10.

Asselin *et al.* [19] introduced a White-type multireflection set-up. While this design offers a really stable and easy way to provide an important number of passes, 24 in the present case, the main drawback is that the jet is crossed at different positions and so different temperature regions are probed. However, according to these authors, the separation between the first and last light spots varies by about 8 mm along the jet axis, reducing this problem.

Another strategy was recently proposed by Petry *et al.* [61] who designed a very compact cell allowing 11 passes through a jet with an experimental gain of 10.3 in

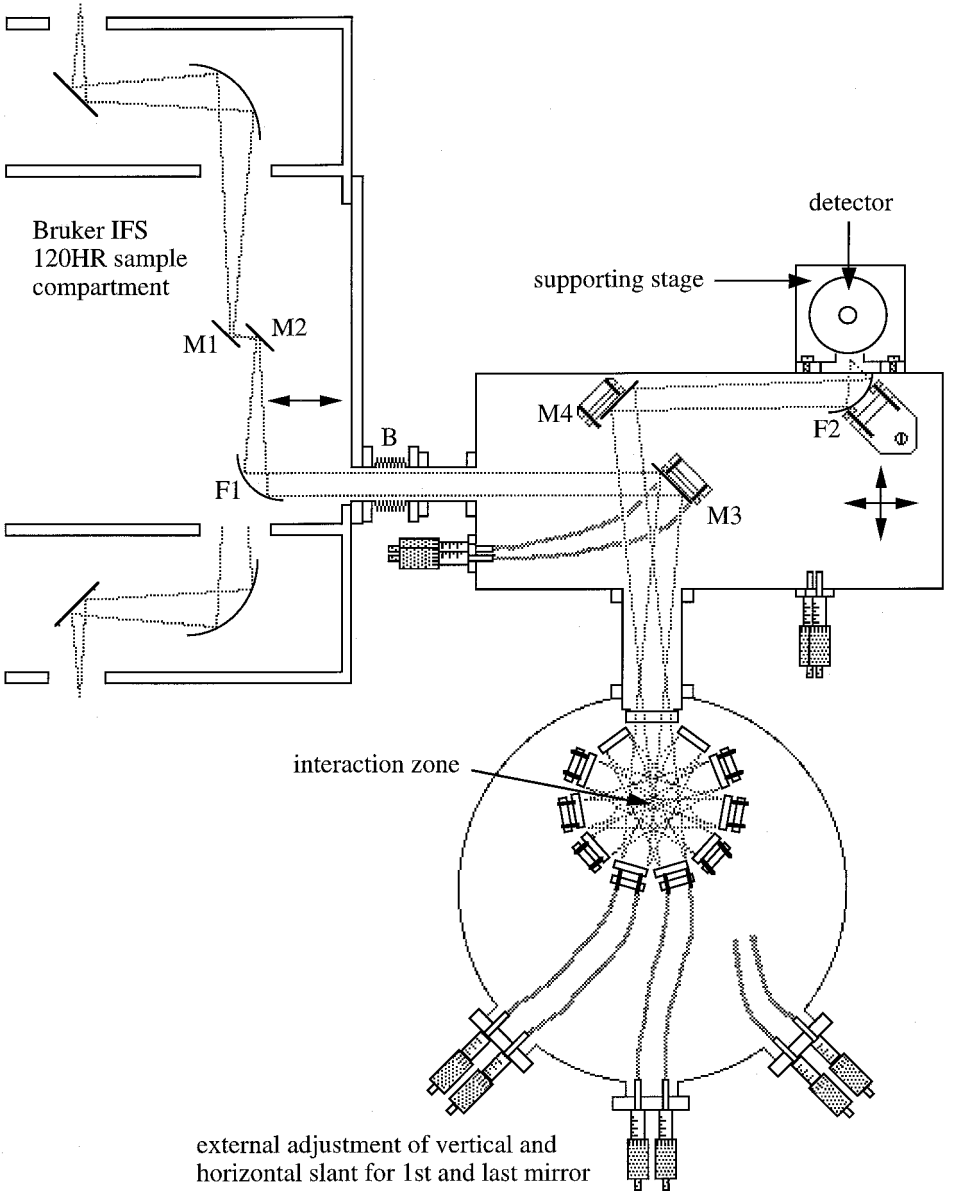

Figure 9. Schematic view of the star-like jet FT spectrometer set-up at Monash (with permission from the authors, adapted from [18]).

sensitivity. Figure 10 presents a schematic of the optical set-up. The design is based on two spherical mirrors. The parallel light beam from the spectrometer is focused on a small aperture in the first mirror. After 10 reflections, the beam is refocused on a hole in the second mirror and leaves the cell. The waist that is generated in the centre of the cell is about 10 mm wide, which is suitable to allow either pinhole or small slit jets to be probed. A detailed discussion of the image formation is given by Gross *et al.* [129].

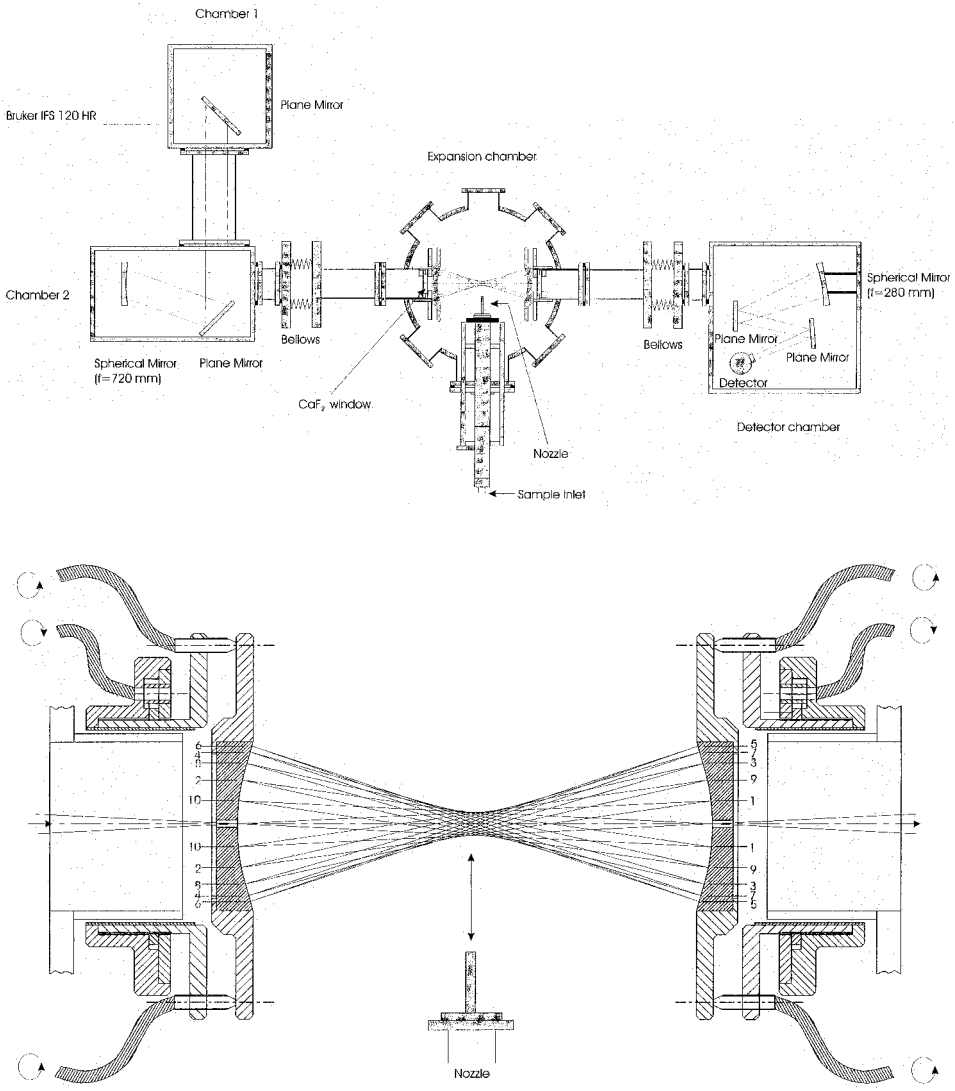

Figure 10. Schematic view of the multi-pass FT spectrometer set-up at Giessen (unpublished results from [61], with permission from the authors, Giessen data); top: general view; bottom: details of the optics.

Due to the flexibility of the original design of the jet system [15] the multireflection unit could be added with no modifications to the system other than some adjustments of movable parts. This design is very compact and quite ingenious. However, it is not versatile in the sense that the arrangement must be calculated by a ray-tracing program in order to determine the exact mirror distance d and cannot be later modified.

The optics designed by Asselin *et al.* [19] and by Petry *et al.* [61] also can both be used with small slits, as the authors report. Slit jets are further described in section 3.4.

3.3. *Multinozzle assembly*

The multinozzle system is achieved by multiplying the number of pinholes over one single light pass. This approach was implemented at ULB, following a suggestion by Jost (Laboratoire des Champs Magnétiques Intenses, Grenoble) [130], and is described in [105] (see also [78]). The system consists of a series of 400 μm diameter pinholes mechanically drilled in an 18 cm long aluminium plate separating the gas reservoir and the vacuum chamber. Various plates with different numbers of equidistant holes were tested up to a maximum of 31 holes, as imposed by the available pumping system. As assumed in the numerical study of a free jet multinozzle source published by Kuleznev *et al.* [131], one can expect the neighbouring expansions to interfere, defining a more complex shock wave pattern than described in the previous section.

The Ar^+ laser induced fluorescence of NO_2 in the visible spectral range was used to visualize the flow structure in the ULB multinozzle assembly [132]. An expansion of NO_2 and argon mixed in equal amounts was formed using standard working conditions (T_0 = 300 K, p_0 = 100 kPa, p_r = 50 Pa). The flow was then excited using an Ar^+ continuous-wave (cw) laser (5 W, all lines). The laser beam was set parallel to the hole alignment and positioned 6 mm (δ_{light} = 15) below the nozzle exits. This positioning corresponds to that for the FT light beam under normal working conditions. In this experiment, the 'hydrodynamic' time† defined as the time needed by the molecules to 'fly' through the silence zone can be estimated to few tens of microseconds while the lifetime of the excited NO_2 molecule is typically of the order of 20 μs [133]. Thus, the NO_2 fluorescence allows the complete structure of the supersonic expansion to be observed.

A section of the 31 pinhole expansion was photographed using a 1/1 macro-objective, as presented in figure 11. The gas expands from the top to the bottom of the picture. The reservoir as well as the pinholes, not directly visible on the picture, are depicted using white hatched marks. The two circular shadows appearing on each side of the picture are screws used to hold the aluminium plate on the reservoir and are not relevant to the present discussion. Graph paper placed behind the expansion appearing in the background of figure 11 allows the various observed features to be scaled down.

Various well separated zones can be observed. The most luminous zones, in yellow, presenting the shape of inverted triangles, are centred on each gas exhaust, 5 mm away from its first neighbour. Thus, each triangle represents a multinozzle silence zone, containing the cold gas with $M \gg 1$. This triangular shape does not match the standard or 'academic' single pinhole expansion shape depicted in figure 5. It is believed that two nearby barrel shocks do cross each other and define this oblique shock wave structure observed in the picture. It can be expected that, when crossing these shock waves, the flow suffers sudden thermodynamic change, involving important warming, in particular.

A second important feature, highlighted by yellow dots on figure 11, is the tenuous line appearing below the triangles, stretching from one side of the expansion to the other. This line marks the end of the NO_2 fluorescence zone and is interpreted

† The hydrodynamic time can be defined as $\tau_{hyd} = x_M / u_{max}$, where x_M is the Mach disc location of a single pinhole expansion given by equation (16), and u_{max} is the maximum flow velocity calculated from equation (4), using $\gamma_{mix} \approx 1.4$ calculated from equation (11). Finally, one finds u_{max} = 659 m s^{-1}, x_M = 12 mm and τ_{hyd} = 18 μs.

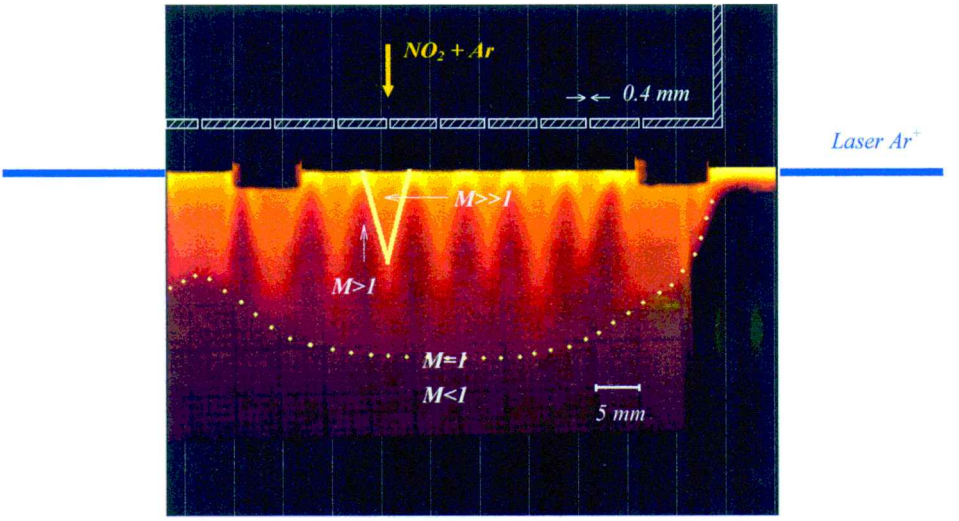

Figure 11. Picture of a portion of the multinozzle assembly used at ULB and described in [105]. The jet-geometry, including the location of the normal shock, is visualized through the Ar^+ laser induced fluorescence in NO_2 flowing in the expansion (M = Mach number).

as the normal shock wave on the residual background pressure. The second law of thermodynamics requires that such a shock wave produce a change from supersonic to subsonic regimes. Thus the regions located above and below (on the picture) the normal shock wave correspond to $M > 1$ and $M < 1$, respectively.

This 'visual' analysis of the flow structure was improved at ULB by recording N_2O FT absorption spectra in the infrared range. N_2O was preferred to NO_2 in these additional experiments because it gives a strong and simple infrared absorption spectrum. The same pressure conditions as for NO_2 were used to keep the same overall expansion pattern. The rotational temperatures were extracted from the intensity ratio of the observed rotational lines, using conventional techniques (see e.g. [107]). Two rotational temperatures were obtained: 44 K ($T_{rot,1}$) and 211 K ($T_{rot,2}$). The colder temperature is assumed to correspond to the 31 adjacent silence zones. A reasonable hypothesis would be to attribute the warmer temperature to the flow located between two consecutive silence zones, thus characterizing molecules that went through the oblique shock wave.

This warming can also be estimated using a relation [55] linking the translational temperatures just before, T_1, and after, T_2, a shock wave:

$$\frac{T_2}{T_1} = 1 + \frac{2(\gamma - 1)}{(\gamma + 1)^2} \frac{M_1^2 - 1}{M_1^2} (\gamma M_1^2 + 1), \tag{19}$$

with M_1 the local Mach number of the flow just located before the shock. Equation (19), which is valid for a normal shock wave, must be corrected in the present case to account for the oblique shockwave arising from the crossing of two nearby expansions. The related streamlines thus intersect the shock with an incident angle β. Assuming that the velocity component of the flow parallel to the shock surface remains unmodified by the shock [55], one has only to consider the velocity

component perpendicular to the shock $u_{1\perp} = u_1/\sin\beta$, used to define the following Mach number:

$$M_{1\perp} = M_1 \sin\beta = \frac{u_{1\perp}}{a_1}. \tag{20}$$

The subscript 1 denotes the flow conditions just before the shock. At $\delta = \delta_{\text{light}}$ the incident angle β measured on the photograph of figure 11 appears to be close to 45°. Using, on the other hand, equation (17) with $\gamma_{N_2O} \approx 9/7$, one finds $M_1(\delta_{\text{light}}) = 8.3$ and then $M_{1\perp}(\delta_{\text{light}}) = 5.9$. Thus, applying equation (19) by replacing M_1 with $M_{1\perp}$ and using the numerical values just mentioned, one finds a temperature ratio of $T_2/T_1 = 5.8$. This value is in reasonable agreement with the one extracted from the N_2O measurements ($T_{\text{rot},1} = 44$ K and $T_{\text{rot},2} = 211$ K), i.e. $T_{\text{rot},2}/T_{\text{rot},1} = 4.8$.

We therefore tentatively suggest that two supersonic zones coexist when the expansions from neighbouring nozzles cross in the multinozzle system, each of them being characterized by a different temperature.

It was experimentally checked [132] that by increasing the distance between two adjacent pinholes, the jet interferences vanish and each pinhole progressively recovers its individual shock wave pattern. The spatial zones located between two adjacent expansions are then subsonic and contain fully re-thermalized, warm gas (300 K).

The multinozzle system, among other experiments referred to in section 4, was used to investigate the CH_4 absorption spectrum in the 4000–6100 cm^{-1} energy range [64]. However, so far, none of the reported experiments made specific use of the peculiar multinozzle shock wave pattern.

3.4. *Slit jets*

The number of molecules flowing per unit time through a nozzle is proportional to the product p_0A^* (see equation (14)). In order to raise the flow rate, one can either increase the throat area or the stagnation pressure. In practice, as the reservoir pressure is limited in standard working conditions to a few atmospheres, one eventually enlarges the throat area, using slit nozzles. Such a design is particularly adapted to large pumping capacities, such as produced by root blowers. Planar slit gas sources are currently interfaced to FTS (e.g. [15, 19, 45, 59, 103, 111, 116]). The slit nozzle areas (A^*) reported in the FT–jet literature vary between 0.015 mm^2 [59] to 4.8 mm^2 [106].

The evolution of the Mach number versus the distance after the aperture is given by equations (17) and (18), now using $j = 2$. It can be seen from figure 6 that the Mach number changes more slowly with a slit jet than with a pinhole jet. As a consequence, the rate of fall of the translational temperature with δ is smaller for a slit. The density also decreases more slowly. It can be seen from equations (9) and (17) that the density decrease is now, theoretically, inversely proportional to δ, compared to $1/\delta^2$ for the circular nozzle. The expansion is slower [48] and the number of two-body, and, actually, also of three-body collisions is larger along the expansion. As a result of the two-body collisions, mainly, the internal degrees of freedom of the molecules (rotation, vibration) have a greater opportunity to equilibrate with the translational temperature [56]. As a consequence of the three-body collisions, molecular complexes are more easily formed. Bevan and co-workers [17, 45, 113–115, 134] and, more recently, Suhm and co-workers [22], used slit nozzles extensively to form and observe complexes of various sizes.

From the flow velocity (equation (10)) and the related temperature evolution

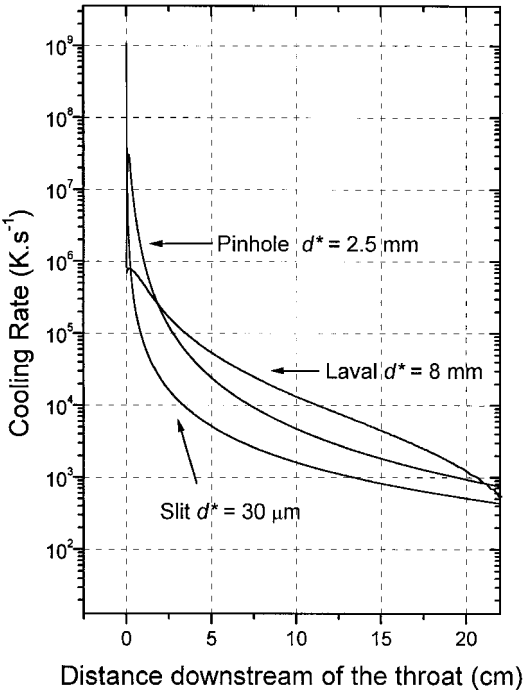

Figure 12. Cooling rates associated with pinhole, slit and Laval expansions. The calculations were performed by considering a pure argon expansion and a reservoir temperature of 300 K.

along the jet axis (equation (8)), one can calculate the cooling rate using [48]:

$$-\frac{\mathrm{d}T}{\mathrm{d}t} = -u(x)\frac{\mathrm{d}T}{\mathrm{d}x} = -\frac{u_{\max}}{d^*}\frac{T}{\delta}(3-j)(\gamma-1). \tag{21}$$

As an illustration, we performed calculations using both a 30 µm × 160 mm slit, which is the size of the ULB design [106], and a 2.5 mm diameter pinhole nozzle, thus of equivalent area and therefore flow rate. Figure 12 shows the related cooling rates. The rate appears to be much higher initially for the slit jet, because of the $1/d^*$ dependence in equation (21). At longer distances, however, the pinhole cooling rate becomes about one order of magnitude more efficient.

Concerning the flow structure of a slit expansion, one can refer to the work done by Dupeyrat [135]. This bi-dimensional problem leads to the more complex shock wave pattern that is presented in figure 5. The silence zone is encapsulated in a system of lateral shocks either converging or diverging. The latter can only be visualized from a side view. The converging shocks intersect below the orifice at a position δ_L given by the empirical relation:

$$\delta_L = \frac{x_L}{d^*} = 40\left(\frac{p_0}{p_r}\right)^{0.34}. \tag{22}$$

As explained in the previous section, the flow is abruptly slowed down after crossing the lateral shock waves but still remains supersonic. The transition between supersonic and subsonic regimes occurs after crossing a normal shock wave whose

position is assumed to obey this other empirical relation:

$$\delta_M = \frac{x_M}{d^*} = 1.23 \left(\frac{p_0}{p_r}\right)^{0.775}. \tag{23}$$

It can be seen from equation (23) that for a given pumping speed, and hence a precise nozzle flow rate and a precise pressure ratio, the normal shock wave can be moved away from the gas exit by increasing the slit width, and decreasing the slit length to keep the same aperture area.

Last but not least, the reduced flow divergence of a slit expansion leads to a reduced Doppler line broadening of interest for high-resolution spectroscopy. Hepp *et al.* [44] report a linewidth of 0.0034 cm^{-1} (FWHM) measured in an expansion of methane seeded in argon (see figure 3), while Walters *et al.* [15] measured the Doppler broadening in a CO_2 expansion probed in directions parallel and perpendicular to the slit length and found 0.003 cm^{-1} (FWHM) and 0.006 cm^{-1} (FWHM), respectively.

In the case of slit nozzles, optical problems arise because of the difficulty of getting a quasi parallel beam of light with a narrow waist and a small divergence, to fit the expansion size along the slit. The beam emerging from the spectrometer can usually be made parallel, using commercial optics provided by the manufacturer. It is, however, of large diameter and effort must be made to shape the beam in a converging pattern so that the focal point is located in the region of the expansion to be explored. The divergence of the resulting beam must be relatively small to limit the problems raised by the averaging of the temperature gradient of the jet. In practice, one has therefore to work with relatively long focus optics, as achieved by Bevan and co-workers (see figure 2.3 of [134] for a schematic description of their set-up). The problem was even more dramatic in the set-up of Georges *et al.* [105] who used a focusing mirror of a focal length of 1315 mm to probe a section about 16 cm long in the expansion formed either in the multinozzle design described in the previous section, or in a long slit. In such an arrangement, the beam is 7 mm wide at the cell windows, located close to the expansion, and 5 mm wide at the focus point. Note also that the choice of the type of mirror is critical when dealing with optical correctness of the beam (astigmatism, aberration) in the path from the spectrometer to the detector located behind the expansion cell, and thus outside from the spectrometer. Elliptic and parabolic sections are commonly used to account for these problems. It is likely that toroidal sections, leading to a significant decrease in the number of required mirrors, may provide an interesting alternative.

Figure 13 presents a schematic view of the set-up at ULB [107], which incorporates either a long slit or a multinozzle expansion. The multinozzle system, as well as some of the available slits, in brass, can be heated up (see figure 16 in section 4). The expansion section mounted directly on top of the pumping units is located some 2 m above the ground and about 1 m above the spectrometer plane. It is vertical, although the whole set-up looks flat on the figure. The light beam emerging from the spectrometer is thus initially sent vertically up by the first mirror (Mp) and then horizontally to cross the expansion along the slit. This set-up, thanks to the long absorption path (16 cm) and to the large pumping capacity (4000 $m^3\ h^{-1}$) allowing high densities in the expansion, provides boosted sensitivity, however at some expense. It needs rather heavy mechanical and optical designs, it requires a long optical path in free air, thus impeding access to certain spectral regions where

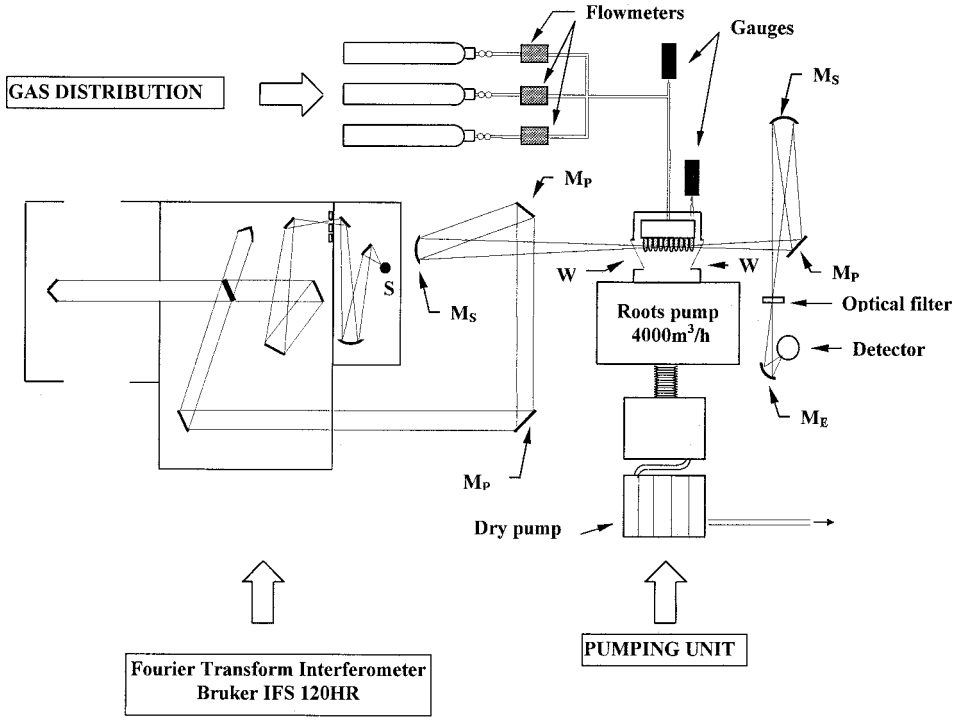

Figure 13. Schematic view of the slit-jet FTS set-up at ULB, adapted from [107]. (M_P: planar mirror; M_S: spherical mirror; M_E: elliptical mirror; S: source; W: CaF_2 window.)

water or carbon dioxide absorbs, and it consumes gas at a great rate, as already pointed out.

3.5. *Confining flow nozzles*

The sharp-edged orifices (pinholes and slits) we have discussed in the previous sections enter the sonic nozzles category, with the $M = 1$ stream section assumed to coincide with the nozzle exit plane. They produce 'free' or 'under-expanded' jets. The latter are so-called because the static pressure of the flow just after the nozzle exit is larger than the static pressure of the chamber in which it propagates.

Nozzles with solid boundaries also exist and are relevant to the present review. The area–velocity relation (equation (12)) shows that the geometrical profile of the channel can be chosen to constrain the flow parameters to pre-selected values. Such constraints can be achieved using conical or Laval nozzles, all of them being either axisymmetric or planar.

Real gases introduce some changes to the ideal isentropic description of free-jets we have so far presented (see e.g. the section 'Non-Idealities in Real Nozzles' in [136]). Viscosity effects induce a reduction of the isentropic flow diameter by developing a boundary layer at the wall. The isentropic core is thus characterized by an effective throat diameter d^*_{ise} smaller than the true geometrical diameter d^*. The viscosity is also partly responsible for bending the sonic surface out of the plane of the throat. Actually, all points at which the flow velocity is sonic define a concave rather than a planar surface, with respect to the flowing direction [82].

The inclusion of a converging nozzle before the throat allows the gas velocity to be progressively adjusted to the decreasing nozzle area and thus to remain uniform over the whole flow area. The sonic surface is then planar and exactly located at the throat cross-section. Moreover, with such a converging nozzle design the isentropic flow diameter is very close to the geometrical throat diameter. Note that the downstream part of the flow is set to expand freely through the vacuum chamber and remains therefore correctly described by the isentropic free-jet model we have used in the previous sections, as shown by Murphy and Miller [137].

In the same way, capillary tubes may be seen as particular kinds of converging nozzles with an infinitely large radius of wall curvature. Some with length-to-diameter ratios between 50 and 200 were reported in the FT–jet literature [19]. The main interest in capillaries is to enhance clustering effects, probably at the early stages of the expansion formation, inside the tube, and before the exit. The density is still high enough to permit a large number of molecular collisions [136, 137]. In general, the inclusion of diverging sections after the throat is a very powerful way to extend clustering in jets because the diverging nozzle lengthens the period during which the flow remains confined, as also evidenced with SF_6 nucleation experiments [138]. The presence of solid boundaries controls the expansion and leads to very low cooling rates not affordable in free jet expansions (see figure 12). Moreover, as pointed out in [112], the use of a diverging nozzle reduces the divergence of the supersonic expansion, limiting the gradient density responsible for anomalous line intensities reported in the FT spectra of free jets [15].

In a recent contribution, Tanimura *et al.* [139] measured the onset of UF_6 nucleation. The $(UF_6)_n$ aggregates were formed by using small bi-dimensional (planar exit) converging–diverging (conical) nozzles and monitored by FT spectroscopy. In these experiments the infrared light beam probes the supersonic flow perpendicularly and before the nozzle exit through windows inserted in the lateral nozzle walls. Due to the confining walls, the flow is one-dimensional and uniform over the whole probed cross-section, as well as presenting precisely defined thermodynamic (static pressure and temperature) and kinetic conditions (cooling rate).

The axisymmetric contoured Laval nozzles, used for decades by aerodynamicists, provide an interesting alternative to free jets, when coupled to FTS. The geometrical profiles of such nozzles are carefully calculated [140] and precisely machined to produce a one-dimensional uniform supersonic flow, that is without gradients, over a length of several tens of centimetres after the nozzle exit. Under such conditions, a cylinder of a few tens of millimetres in diameter, forming the isentropic core in which the conditions are uniform and thermodynamically well defined, is surrounded by boundary layers arising from the viscosity forces of the ambient residual gas chamber. The working conditions, the temperature in particular, can be imposed by profiling adequate supersonic Laval nozzles. However, the boundary layers that develop at the nozzle walls can drastically reduce the isentropic core diameter and limit the spectroscopic applications. The ratio of boundary layer thickness Δ to isentropic core diameter is given by:

$$\frac{\Delta}{d_{\text{ise}}} \propto \frac{1}{(\text{Re})^{1/2}}, \tag{24}$$

with $\text{Re} = \rho u d / \mu$ the dimensionless Reynolds number defined as the ratio of inertial forces to viscous forces, where μ is the viscosity of the gas and d is the diameter of a nozzle cross-section. Equation (24) shows that the boundary layer thickness

is reduced at high Reynolds number. If one expresses the Reynolds number by introducing the mass flow rate (equation (14)), equation (24) can be rewritten as:

$$\frac{\Delta}{d_{\text{eff}}} \propto \left(\frac{\mu d}{\dot{m}}\right)^{1/2}. \tag{25}$$

Equation (25) shows that the isentropic core diameter is preserved if the mass flow rate is kept as high as possible, thus allowing spectroscopic experiments to be performed. Benidar *et al.* interfaced such a uniform flow to a Fourier transform spectrometer and observed the absorption spectrum of the NO dimer [20] (see later figure 21). The Laval nozzles they used have a throat diameter of about 8 mm and the reported effective pumping speed is 22 000 $m^3\ h^{-1}$ atm in argon.

If, compared to pinholes, slit nozzles offer a longer absorption path because the expansion can be probed over the full slit length, another way to increase the absorption path is to probe the expansion along its path, thus making the light and the jet axis coincide. Such a design involves complex transfer optics as well as stable conditions in the expansion over a long pathlength. The use of the Laval nozzles we have just discussed in this section, involving huge pumping units as reported in section 2, provides such an alternative. This design is being developed with success by Georges and co-workers [20], leading to some 36 cm absorption pathlength.

4. Spectroscopic investigations

4.1. *Literature review*

The development of FTIR absorption spectroscopy of jet-cooled molecules can be followed in the literature through papers published by a number of contributing research groups. These papers are listed according to the chronology of the initial or sometimes unique contribution of each group, whose publication date is mentioned: *Yale* in 1981 [9, 84], *ETH-Zürich* in 1984 [13, 57, 59, 67], *Waterloo* in 1986 [111], *National Research Council of Canada* in 1988 [127] and another group in *Waterloo* in 1989 [141], *Cambridge* in 1990 [122], *Giessen* in 1991 [15, 61], *ULB* in 1992 [16, 44, 105, 107], *Sussex* in 1993 (see [142]), *Texas A&M* in 1993 [17], *Rutherford Appleton Laboratory* in 1993 [83], *Tsukuba* in 1993 [143], *Monash* in 1994 [18], *Paris VI* in 1996 [19], *Riken* in 1996 [139] and *Boulder* in 1996 [123]. In this list, the first paper referred to corresponds to the initial contribution of each research group mentioned, and the next ones to any subsequent relevant technical description, sometimes accounting for important modifications in the respective set-ups. Many of these groups are still active in the field and, as pointed out in the introduction, others, such as at *Rennes* [20] and *Göttingen* [21, 22], have just started or, as *Orsay* [23], are planning to contribute.

The following target molecules, investigated in the literature and dedicated to absorption studies in the infrared range, are listed by increasing number of constitutent atoms: DCl [144], CO [18, 59, 112, 144], NO [16, 59], CO_2 [13–16, 19, 83], N_2O [18, 67, 105, 127, 145], NO_2 [16, 26, 28, 29, 83, 123], C_2H_2 [59], NH_3 [9, 67], CH_4 [13, 59, 64, 67], CH_3Cl [13, 59, 64, 67, 84], CHF_3 [59, 92], $CHClF_2$ [97], $CHCl_2F$ [98, 146], CCl_2F_2 [18, 86], $CBrF_3$ [145], $CBrClF_2$ [86, 88], CF_3Cl [58], CF_3I [93, 95, 145], CCl_3F [99], NCCNO [61], C_2H_4 [102, 103, 107], CH_3OH [44], CH_3C_2H [59], CH_3CHO [110, 147], C_5O_2 [61], C_2H_6 [44, 108, 109, 142, 148, 149], C_2F_6 [143], CH_3CHF_2 [87, 150], CH_3CF_2Cl [151], CH_2ClCH_2Cl [62], CF_3CH_2F [85], C_3H_6 [152], $(CH_3)_2O$ [153], C_4H_5N [154], C_3F_7H [87, 155], C_5H_5N [90], C_6H_6 [89], C_5H_8 [156]. Heavier stable species were studied, SF_6 [104, 111], ReF_6 [157] and metal

carbonyl compounds, $Ni(CO)_4$ [19, 122], $Fe(CO)_5$ [19] and $Mo(CO)_6$ [158]. Some contributions concern unstable species: SPF_3 [94] and C_3O_2 [15]. Complexes were investigated, some of which are NO and/or NO_2 containing species, namely $(NO)_2$ [20, 101], N_2O_3 [106] and N_2O_4 [16, 26–29], as well as HCl-containing molecules [17, 45, 113–115]. Larger clusters presenting almost unstructured spectral signatures, made of CO_2 [14], N_2O [22, 105, 127], HF [67, 69, 96, 159], containing HF or HCl [22, 100, 160], and made of larger species [21, 22, 111, 139, 161], were also studied.

FT–jet work was also carried out to record, in absorption or in emission, the fine structure of electronic transitions. In absorption, NO_2 [123] and ClO_2 [125, 126, 162] were investigated. In emission, the literature mentions CH [79, 163], C_2 [121], CN [114, 119, 120, 124, 128], CCl [117], N_2 [164–166], NO [167, 168] and I_2 [169], CCN [118], $CuCl_2$ [170], CH_3N [116, 171] and larger polyatomic radicals, *p*-xylyl [172] and $C_6H_3F_3^+$ [173]. Emission between vibrational states within the ground electronic state was also observed using FTS, already in 1981, in jet-cooled CO and CO_2 [174–176]. We have included the studies just mentioned in separate sections of table 3, for completeness, although the present review is mostly devoted to high resolution infrared absorption spectroscopy. Studies by Leone and co-workers, recording time-resolved emission spectra using FTIR under quasi jet-cooled conditions are to be mentioned (see e.g. [78, 177] and references therein) but are not listed in table 3. This table updates previous review papers [11, 45, 134, 178–180].

In order to provide an entry into the literature complementary to table 3, we list hereafter, using the same ordering for the groups as previously in this section, all references for those groups having published two or more papers in the field. We are restricting the selection listed to higher resolution absorption investigations in the infrared range: *Yale* [9, 84, 89, 90], *ETH-Zürich* [13, 28, 29, 57–59, 67, 92–99, 145, 146, 157, 179], *Giessen* [15, 61, 144], *ULB* [11, 16, 26, 27, 44, 62, 64, 102–110, 142, 147–149, 152–154], *Texas A&M* [17, 45, 113–115, 134], *Monash* [18, 85–88, 142, 150, 151, 155], and *Paris VI* [19, 100, 101, 156, 158].

In the next two sections, we emphasize a number of studies, in particular those related to the ULB investigations.

4.2. *High resolution infrared study of hydrocarbons*

Most of the investigations listed in table 3 are devoted to stable species, hydrocarbons in particular. We already highlighted in section 2.3 experiments aimed at the study of the relaxation between levels with different nuclear spin statistics. In most papers, however, it is the spectral decongestion resulting from the decrease of the rotational temperature in the expansion that is exploited to unravel the fine structure of the recorded bands, allowing in many cases their rotational analysis to be performed for the first time. In this category are the ULB studies in the mid and near infrared ranges of ethylene (C_2H_4) [102, 103, 107] and ethane (C_2H_6) [44, 108, 109, 142, 148, 149], which are highlighted hereafter.

Ethylene in the ground electronic state is a planar species (D_{2h} symmetry) exhibiting a dense vibration–rotation spectrum. The study of this species using FT–jet experiments was quite challenging as most of the bands in the lower infrared range were already studied at high resolution (see [181] for a review of the literature). In the overtone range, on the other hand, one had to face the usual severe decrease in the band strength occurring for overtone and combination absorption bands compared to fundamental bands. The input of the FT–jet data helped at three different levels.

Table 3. Species studied in the literature using FT–jet experimental set-ups, grouped in sections (I to IV) according to the nature of the investigation. In section I, concerning infrared absorption studies, the molecules are gathered roughly in chemical families. All singular species in that section are listed in the first of these groups.

	Species[a,b]	Resolution (cm^{-1})[c]	Temperature (K)[d]	Band (spectral range) (cm^{-1})	Major focus[b]	References
I	RV absorption					
	DCl	0.0023	12	1–0 (2110)	R Cooling	[144]
	NH_3	0.01–0.06	100	ν_2 (970)	NSS relaxation	[9, 67, 96]
	NCCNO	0.008	7	Various bands (1000–2500)	R analysis	[61]
	SPF_3	0.004	80	ν_1 (980)	R analysis	[94]
	CO	0.0023–0.5	5.9–100	1–0 (2000)	R cooling	[18, 57 59, 111, 112, 144]
	CO_2	0.004–0.15	4–36	ν_3 (2350)	R cooling	[13, 15, 16 19, 83]
	C_3O_2	0.008	60	ν_7 (2290)	R analysis	[15]
	C_5O_2	0.008	13	Various bands (1500–2500)	R analysis	[61]
	NO	0.004	17; $T_e \sim 50$	1–0 (1880)	E cooling	[16, 59]
	$(NO)_2$	0.006	4	ν_1/ν_5 (1800)	Observation	[20, 101]
	N_2O	0.004–0.01	6–26; $T_{vib} \sim 180$	Various bands (1300–4800)	R/V cooling	[18, 67, 105, 145]
	NO_2	0.0024–0.1	20–200	Various bands (700–3300)	Abundance measurements	[16, 26, 28 29, 83, 123]
	N_2O_3	0.005	44	ν_1 (1830)	R analysis	[106]
	N_2O_4	0.0024–0.1	30–100	Various bands (700–3300)	R analysis Abundance measurements	[16, 26, 29, 83, 123]
	CH_4	0.00185 –0.015	10–30	Various bands (3000–6000)	NSS relaxation R/V analysis	[13, 44 59, 64]
	CH_3Cl	0.06	120	ν_1; ν_2; ν_3 (700–3000)	R analysis	[84]
	CHF_3	0.004	40	ν_2/ν_5 (1150); CH stretch (3000)	R analysis	[59, 92]

$CHClF_2$	0.004–0.005	50	ν_2; ν_4; ν_3/ν_5 (800–3000)	R analysis	[97, 146]
$CHCl_2F$	0.004	70	Various bands (700–1300)	R analysis	[98]
CCl_2F_2	0.0034	40	ν_1/ν_8 (1100)	R analysis	[18, 86]
$CBrF_3$	0.004	45	ν_1/hot band (1100)	R analysis	[145]
$CBrClF_2$	0.0024	40	Various bands (800–1200)	R/V analysis	[86, 88]
CF_3Cl	0.005	32; $T_{vib} \sim 240$	ν_1/ν_4/hot band (1200)	R analysis	[58]
CF_3I	0.004–0.005	15–50	$\nu_1/2\nu_5$; ν_4 (1080–1200)	R analysis	[93, 95, 145]
CCl_3F	0.004	20	ν_1 (1100)	R analysis	[99]
C_2H_2	0.01	31	ν_3 (3300)	Relaxation mechanisms	[57, 59]
CH_3C_2H	0.015	45; $T_{vib} \sim 150$	ν_1/hot band (3300)	R/V cooling	[57, 59]
C_2H_4	0.02	36–53	Various bands (3100–7900)	R/V analysis, hot band	[102, 103, 107]
C_2H_6	0.00185 —0.01	40	Various bands (1400–4500)	R/V analysis, hot band	[44, 108, 109 142, 148, 149]
CH_3CHF_2	0.0035–0.1	50	Various bands (650–4500)	R/V analysis	[88, 150]
CH_3CF_2Cl	0.0035–0.1	50	Various bands (650–4500)	Observation	[151]
CH_2ClCH_2Cl	0.01	30	ν_{16}/hot bands (1230)	V/R analysis	[62]
CF_3CH_2F	0.0035	65	ν_{14}; ν_{15} (700; 1300)	R analysis	[86]
C_2F_6	0.2–1	6–65	ν_1; ν_7 (1120; 250)	Test species	[143]
$(CH_3)_2O$	0.01	20	Various bands (900–3000)	R analysis	[153]
CH_3OH	0.01		CH stretch (3000)	Test species	[44]
CH_3CHO	0.01	100	Various bands (700–3300)	R/V analysis	[110, 147]

Table 3 (*cont.*)

Species[a,b]	Resolution (cm^{-1})[c]	Temperature (K)[d]	Band (spectral range) (cm^{-1})	Major focus[b]	References
C_3H_6	0.01	50	ν_{12}/ν_{13} (960)	R analysis	[152]
C_5H_8	0.1		CH stretches (2800–3000)	V analysis	[156]
C_3F_7H	0.0035–0.1		Various bands (650–4500)	Observation	[88, 155]
C_4H_5N	0.01	40	ν_1 (3530)	R analysis	[154]
C_5H_5N	0.06	135	ν_{11} (3060)	Band contours	[90]
C_6H_6	0.06	79	ν_{11}; ν_{20} (670; 3050)	Band contours	[89]
$Ni(CO)_4$	0.004–0.06	6	ν_5 (2050)	Test species	[19, 122]
$Fe(CO)_5$	0.004	4	ν_6 (2000)	R analysis	[19]
$Mo(CO)_6$	0.004	13	ν_6 (2000)	R analysis	[158]
SF_6	0.005	30	$\nu_{12} + \nu_6/\nu_3$ (990)	R analysis	[104]
ReF_6	1	50	ν_3 (720)	R analysis	[157]
HF–CO	0.005	3	ν_1 (3850)	Observation	[45, 114]
$(HF)_n$	1	60	1–0 (3400)	Cluster formation	[60, 69, 96]
HCl–Ar	0.004		ν_1 (2880)	Observation	[114]
$(HCl)_n$	0.007	8–20	ν_1; ν_2; ν_5 (2890; 2840; 2810)	R analysis Cluster formation	[22, 45 113–115]
DCl–DME[e]	0.5		ν_5 (1750–1950)	Observation	[100, 160]
HCl–DME			(2400–2700)		
HCl–CO	0.007	8	ν_1; ν_2 (2150; 2850)	R analysis	[17, 45]
$HCl–N_2$	0.004	15	ν_1 (2870)	R analysis	[114]
$(CO_2)_n$	3		Various bands (600–3800)	Cluster formation	[14]
$(N_2O)_n$	0.04	3	Various bands (1100–3500)	Cluster formation	[22, 105, 127]
$(UF_6)_n$	0.5		ν_3 (630)	Cluster formation	[139]
$(SF_6)_nAr_m$	0.5		ν_3 (950)	Cluster formation	[83, 111]
Organic clusters	0.1		Various ranges	Cluster formation	[21, 22, 161]

II	RV emission					
	CO	0.24	15	1–0 (2100)	Probe of surface reaction	[114, 175]
	CO_2	0.1–0.24		v_3 (2300)	Probe of surface reaction	[174, 176]
III	RVE absorption					
	ClO_2	0.5	15	$\tilde{A}$–$\tilde{X}$ (21 000–33 000)	R/V analysis	[125, 126, 162]
IV	RVE emission					
	CH	0.1		A–X (visible)	Probe of dissociation reaction	[79, 163]
	C_2	0.025	90	d–a (22 800–16 500)	R/V analysis	[121]
	CN	0.01–0.25	32–200 $T_{vib} \sim 2200$	A–X, B–X (38 000–2500)	R/V analysis	[114, 119, 120 124, 128]
	CCl	0.05	30	A–X (36 000)	R analysis	[117]
	N_2	0.05	20	a–a', w–a, C–A (15 000–3500)	R/V analysis	[164–166]
	NO	0.05	20	Various systems (1300–2500)	R/V analysis	[167, 168]
	I_2	0.1	13	A–X	Test species	[169]
	CCN	0.025	30	$\tilde{A}$–$\tilde{X}$ (20 300–19 100)	R/V analysis	[118]
	$CuCl_2$	0.02–0.04	10	$\tilde{A}$–$\tilde{X}$ (17 500–7200)	R/V analysis	[170]
	CH_3N	0.07	12–25	$\tilde{A}$–$\tilde{X}$ (31800)	R analysis	[116, 171]
	p-Xylyl	0.2	45	$\tilde{A}$–$\tilde{X}$ (21 800–20 800)	Band contours V analysis	[172]
	$C_6H_3F_3^+$	0.05	80	$\tilde{B}$–$\tilde{X}$–$\tilde{B}$–$\tilde{A}$ (22 500–21 500)	Band contours V analysis	[173]

[a] Various isotopomers may have been investigated (see references).
[b] R: rotation; V: vibration; E: electronic; NSS: nuclear spin symmetry.
[c] Apodized or non-apodized resolution (with possible differences in the definition of resolution), depending on the author (see references).
[d] Estimated rotational temperature (otherwise specified).
[e] DME: dimethylether.

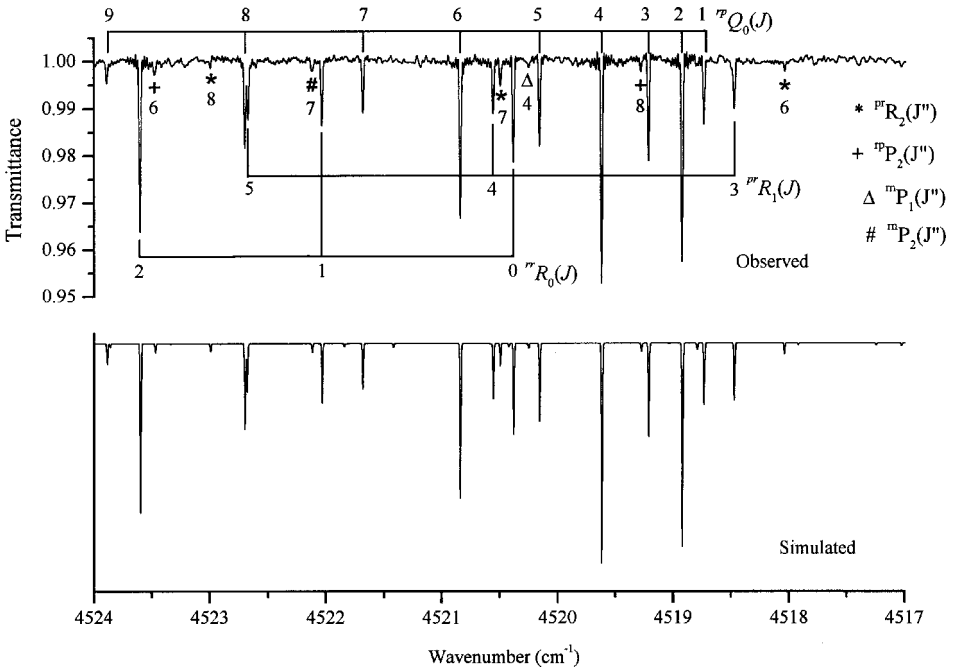

Figure 14. Portion of the jet-cooled (1:1 mixture of $Ar:C_2H_4$, 600 scans, 0.02 cm^{-1} resolution, T_{rot} = 53 K) transmittance spectrum of $^{12}C_2H_4$, in the range of the $\nu_5 + \nu_{12}$ band, recorded using a FT spectrometer and simulated (adapted from [103], ULB data).

In the first place, thanks to the combination of high instrumental resolution (0.01–0.02 cm^{-1}) and efficient spectral decongestion (T_{rot} = 36 or 53 K), the FT–jet data recorded using the 16 cm long slit jet facilities available at ULB [103, 107] allowed vibration–rotation bands to be studied and rotationally assigned for the first time. Figure 14, from [103], exemplifies the rotational analysis of the $\nu_5 + \nu_{12}$ combination band by presenting a 7 cm^{-1} spectral portion of that band (with ν_5 and ν_{12} two of the CH stretching modes, see [181]). The simulation, performed by Perrin (PPM, Orsay) and detailed in [103], accounts for Coriolis resonances and is also presented in figure 14.

In the second place, thanks to the broad coverage provided by FTS, an extended analysis could be performed over the full range between 4100 and 6200 cm^{-1}, only previously studied at low resolution and under room temperature conditions. An overview of the spectra is presented in figure 15. The analysis resulted in extensive information on the vibrational levels of ethylene in this excitation range. This information, concerning *u*-symmetry levels, was combined with the literature results, and allowed the vibrational energy pattern in ethylene to be further studied [181]. New constants of the motion were suggested to deal with the overtone range, along the line of previous investigations in acetylene [11]. Interesting questions, such as the explanation of the relative intensity of all four allowed CH combination bands, one not being observed under these experimental conditions, still remain to be answered.

In the third place, hot bands could be spotted in the 3 μm range, using the following experimental trick. The FT–jet absorption spectrum was recorded twice under identical experimental conditions, similar to those used to record the data

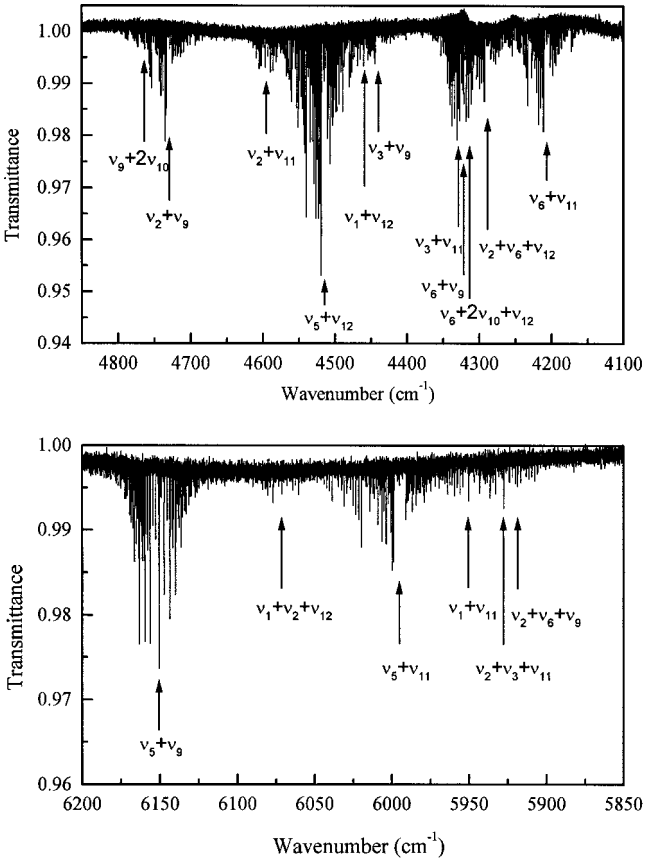

Figure 15. Overview of the jet-cooled (1:1 mixture of Ar:C_2H_4, 600 scans, 0.02 cm^{-1} resolution, T_{rot} = 53 K) transmittance spectrum of $^{12}C_2H_4$, between 4100 and 6200 cm^{-1}, recorded using a FT spectrometer (adapted from [103], ULB data).

presented in figures 14 and 15, using different slit conditions. The difference between the spectra was produced by heating the slit to some 150°C using internal resistors framing the 16 cm slit over its full length, in one of the experiments. The ratio between the two spectra, presented in figure 16, highlights hot bands. The population on a number of excited vibrational levels, ν_{10}, ν_8 and ν_7, respectively lying at 826, 940 and 949 cm^{-1} above the ground state [181], is expected to be increased by the heating procedure and to participate in the hot band absorption. The quality of the data compares reasonably well with the spectra recorded by Reuss and co-workers using collision induced energy population transfers which allowed the rotational analysis of some of these hot bands to be performed [182, 183]. The rotational temperature under the experimental conditions used to record the data presented in figure 16 was about 50 K for the close-lying fundamental bands [102]. The vibrational temperature was not determined.

Ethane is a molecule with two CH_3 internal rotors, whose vibration–rotation spectrum in the ground electronic state is very dense and complex. Besides one fundamental band that could be fully analysed [184], the literature only mentions partial rotational assignments for a very limited number of bands (see [185] for a

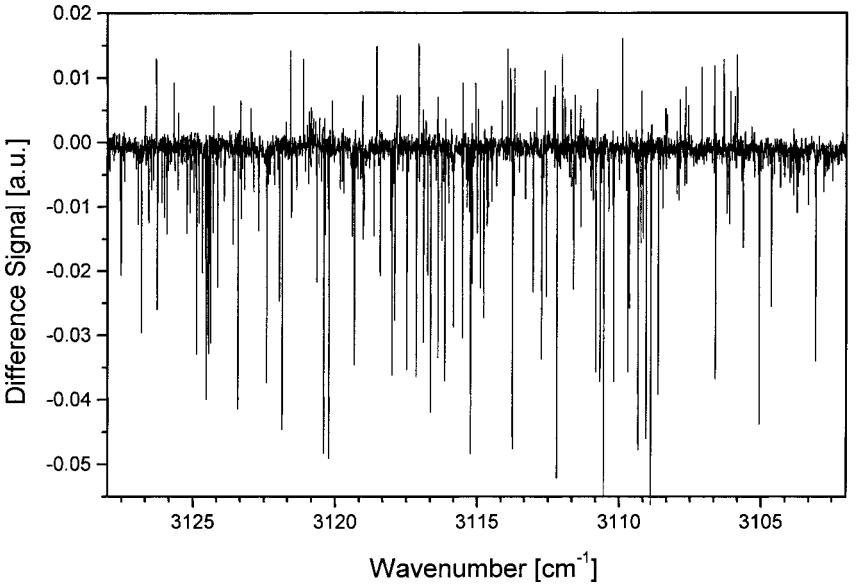

Figure 16. Portion of the difference between the jet-cooled FT absorption spectrum of $^{12}C_2H_4$ in the region of 3000 cm^{-1} recorded with and without a heated (150°C) slit recorded using a FT spectrometer (unpublished results from Herman and co-workers: 1:1 mixture of Ar:C_2H_4, 40 scans, 0.01 cm^{-1} resolution, T_{rot} = 50 K, ULB data).

review of the literature). The same three types of results, as just emphasized for ethylene in the previous paragraph, could be obtained from an extensive FT–jet investigation performed at ULB. Figures 17 and 18 demonstrate the power of such investigations in unravelling a broad spectral range in the overtone region, allowing detailed rotational assignments to be performed. The observation of hot bands was also reported, but is not detailed here [44]. Figure 18 highlights the observation of a band at lower energy, to demonstrate the usefulness of the experiments in the mid-infrared range. In this figure, a band that is hidden in the congested room temperature spectrum is identified in the FT–jet spectrum and could be vibrationally ($\nu_8 + \nu_{12}$) and partly rotationally assigned [149]. Significant progress in the knowledge of the vibration–rotation structure in ethane was made, as summarized in [185]. Compared to ethylene, ethane needs to be further investigated before global models dealing with the vibrational structure can be suggested.

The decongestion ensured by the jet-cooled experimental procedure exemplified in figure 18 was observed in many other investigations reported in table 3 (see also the spectrum of C_5O_2 in figure 22 in the next section). An additional example of spectral decongestion is provided in figure 19, now using a larger metal-containing species. The figure demonstrates the quality of the set-up achieved by the group at Paris VI [158].

4.3. *High resolution infrared study of radicals and unstable species including nitrogen oxides and small molecular complexes*

A large amount of work in the FT–jet literature was devoted to nitrogen oxides. We have presented in figures 1 and 2, in the introduction, some of the results concerning the investigation of the infrared spectrum of N_2O_4. Two major driving

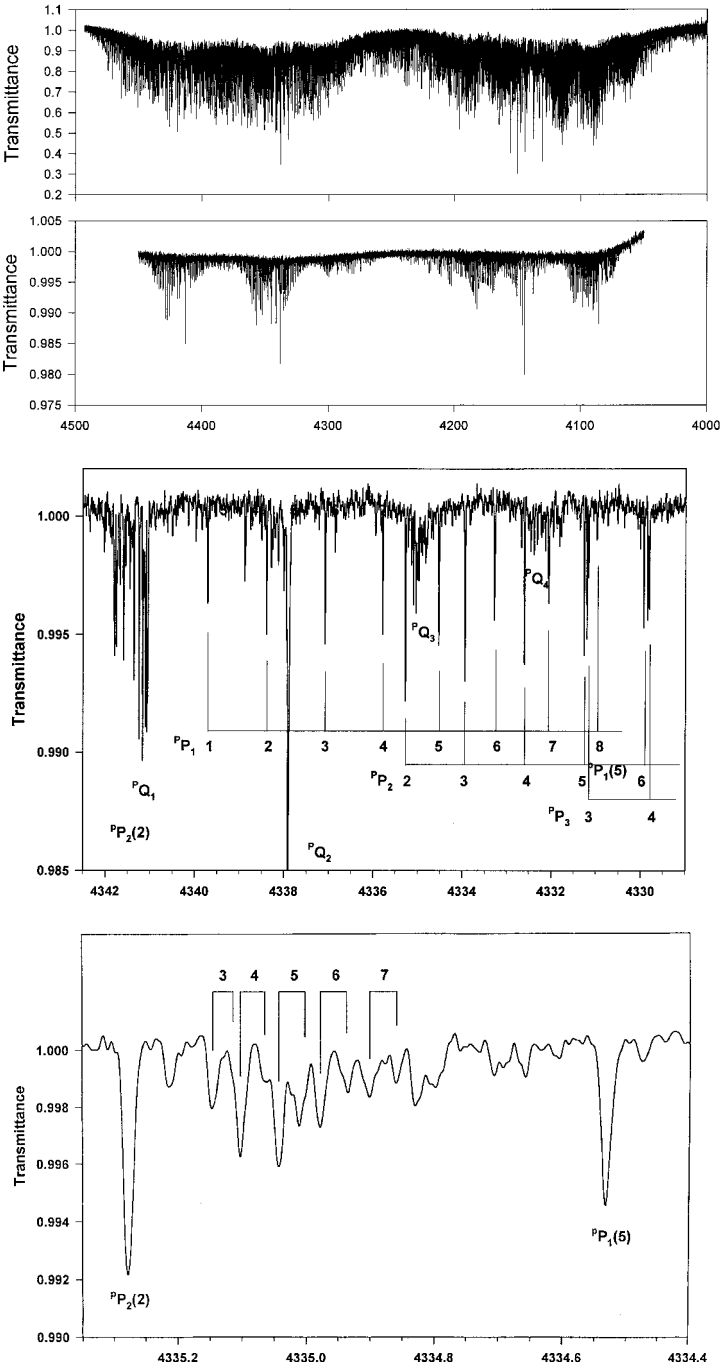

Figure 17. Jet-cooled (1:1 mixture of Ar:C_2H_6, 300 scans, 0.01 cm^{-1} resolution, T_{rot} = 40 K) transmittance spectrum of $^{12}C_2H_6$ in the overtone range recorded using a FT spectrometer (adapted from [108, 109], ULB data). The energy scale corresponds to wavenumbers (in cm^{-1}). Top: overview of the spectrum with, above for comparison, room temperature conditions; middle: details of the $\nu_6 + \nu_{10}$ band showing the first $\Delta K = -1$ subbands; bottom: the torsional splittings in the $^{p}Q_3(J)$ branch of this the $\nu_6 + \nu_{10}$ band, with the stick spectrum simulating approximate relative intensities.

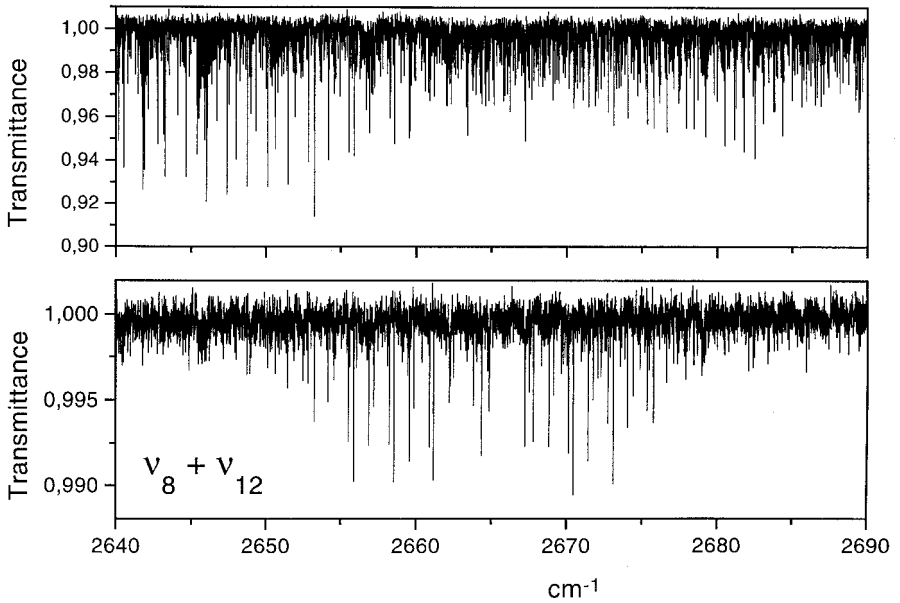

Figure 18. Portion of the jet-cooled (1:1 mixture of Ar:C_2H_6, 200 scans, 0.01 cm^{-1} resolution, T_{rot} = 40 K) transmittance spectrum of $^{12}C_2H_6$ in the fundamental range, compared with the room temperature spectrum, recorded using a FT spectrometer (adapted from [149], ULB data). The energy scale corresponds to wavenumbers (in cm^{-1}).

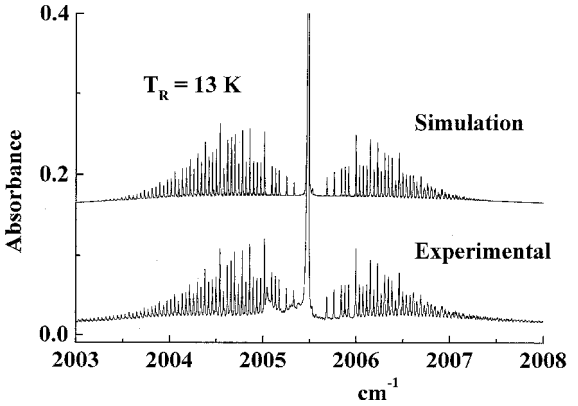

Figure 19. Observed and simulated ν_6 band of $Mo(CO)_6$ recorded under jet-cooled conditions (about 98:2 mixture of Ar:$Mo(CO)_6$, 250 scans, 0.004 cm^{-1} resolution, T_{rot} = 13 K) using a FT spectrometer (adapted from [158], with the permission of the authors, Paris VI data). The energy scale corresponds to wavenumbers (in cm^{-1}).

forces motivate the studies of nitrogen oxides. On the one hand the study of the behaviour of the $NO_2 \leftrightarrow N_2O_4$ chemical equilibrium under jet-cooled conditions is of interest and was attempted by Luckhaus and Quack [28, 29] and by Frost *et al.* [123]. On the other hand, the jet-cooled conditions are known to favour the formation of related dimers and complexes [186] and, at the same time, to allow their otherwise prohibitively dense spectra to be studied.

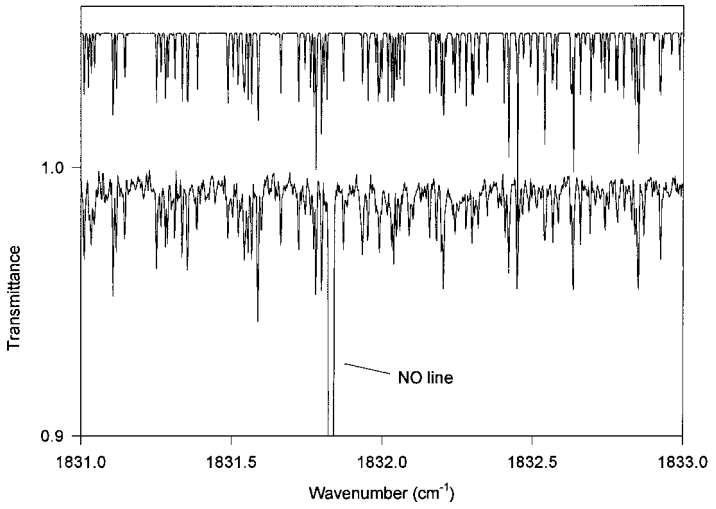

Figure 20. Observed and simulated portion of the ν_1 band of N_2O_3 recorded under jet-cooled conditions (about 1:3 mixture of Ar:NO, 92 scans, 0.005 cm^{-1} resolution, T_{rot} = 44 K) using a FT spectrometer (see [106], ULB data).

The high resolution investigation of the ν_1 quasi diatomic NO-stretch band of N_2O_3 (ON–NO_2) was initiated at ULB using the FT–jet facilities [106], and since significantly extended at Bonn using diode lasers [187]. Figure 20 presents the related FT transmittance spectrum. The observed ON–NO_2 species is planar with the *a* axis directed reasonably close to the direction of the NN chemical bond. Unexpectedly for this NO stretch, the ν_1 induced dipole moment happens to lie close to the direction of this NN bond, as confirmed by *ab initio* calculations [106]. This prediction helped interpreting the absence of a *b*-type subband in the rotational structure of this fundamental band. Although probably searched for by some research groups, the larger complex N_2O_5 has not yet been reported using FT–jet experiments.

The study of the NO dimer, observed and studied using lasers in supersonic jets and using FTS in cooled cells, motivated a number of investigations using FT–jet facilities. These led recently to the observation of the dimer [20, 101], as exemplified in the spectrum recorded at Rennes and presented in figure 21.

Other complexes, containing HF or HCl, were observed and are reported in the literature, from Texas A&M in particular. Very nice data were recorded by this group, which are illustrated in the related references mentioned at the beginning of this section (see table 3) and in an earlier review paper by Arno and Bevan [134].

Two additional examples concerning unstable species are provided by the recent study of C_5O_2 in the Giessen group [61], and the study of SPF_3 at ETH-Zürich in collaboration with Wuppertal [94]. Those investigations are exemplified in figures 22 and 23, respectively. In the case of OC_5O, accumulation of this unstable species in isopropylcyclohexane solution was seeded in 150 hPa argon and its jet spectrum recorded at Giessen. As already pointed out, this spectrum provides another striking example of the use of FT–jet spectroscopy in highlighting bands that can almost not be identified at room temperature, in this case because of the presence of numerous hot bands. In the case of SPF_3, which illustrates the many

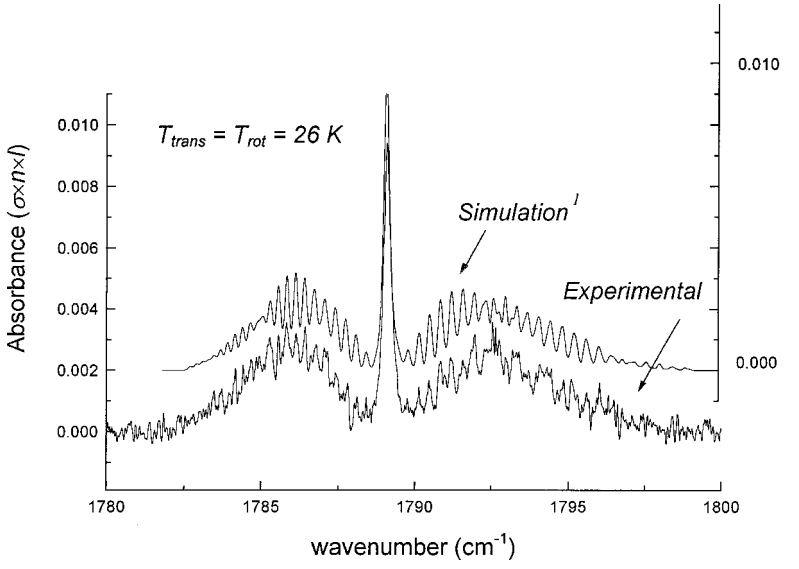

Figure 21. Observed and simulated ν_5 band of $(NO)_2$ recorded under (Laval) jet-cooled conditions (about 19:1 mixture of Ar:NO, 500 scans, 0.05 cm^{-1} resolution, T_{rot} = 26 K) using a FT spectrometer (adapted from [20], Rennes data). The simulation was performed using the rotational constants from [188].

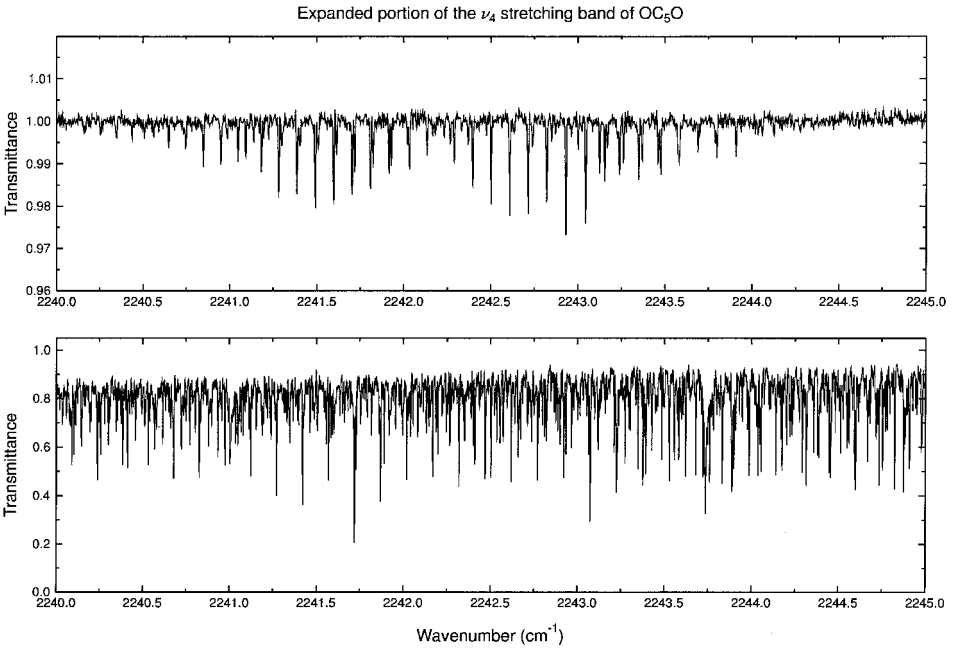

Figure 22. Overview of the ν_4 stretching band of OC_5O recorded under jet cooled conditions (60 scans, 0.008 cm^{-1} resolution) using a FT spectrometer (unpublished results from [61], reproduced with permission from the authors, Giessen data). The lower spectrum corresponds to a cell spectrum with the products of the pyrolysis of the precursors slowly pumped inside, while the upper spectrum was obtained by seeding the same products, after dissolving them for stabilization, in 150 hPa argon and expanded in a jet.

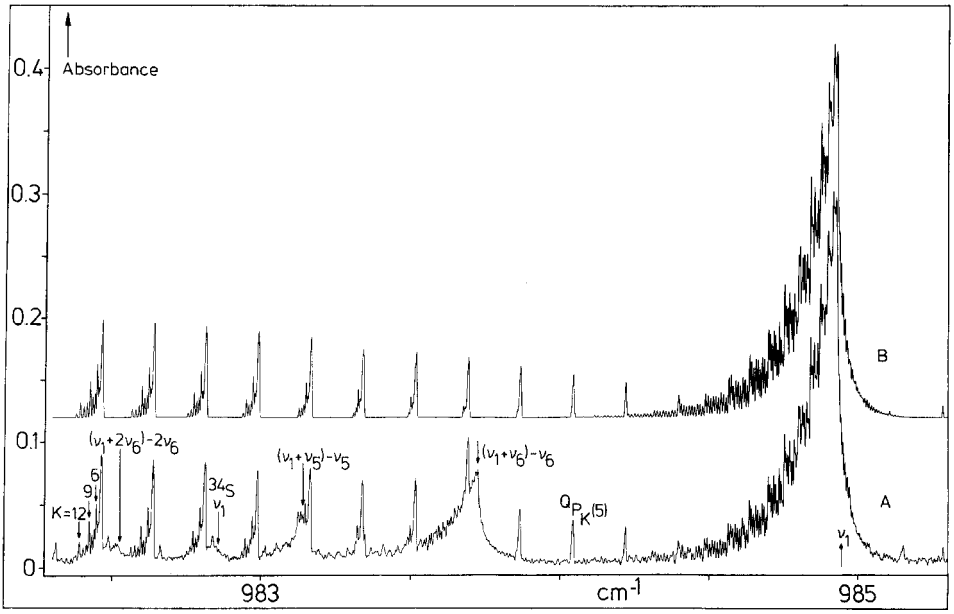

Figure 23. Observed and simulated jet spectrum of SPF_3 close to the ν_1 band centre (neat SPF_3, 0.0024 cm^{-1} resolution, T_{rot} = 80 K) using a FT spectrometer (adapted from [94], with permission from the authors, ETH data). The system allowed recovery of the SPF_3 used in the continuous jet. The energy scale corresponds to wavenumbers (in cm^{-1}).

achievements by the ETH group, the sample was permanently recycled allowing the study to be performed using the FT spectrometer running under continuous operation.

The various studies highlighted in this section thus demonstrate that the basic FT spectrometer characteristics are not incompatible with the investigation of unstable species and of small sized complexes.

4.4. *Trends for high resolution absorption infrared spectroscopy*

The literature review demonstrates that FT–jet spectroscopy today offers a variety of facilities, competing with laser investigations in some cases and providing significant advantages in other cases. A number of additional investigations of what have today become 'conventional' FT–jet studies can therefore be expected to appear in the literature. As far as high resolution instrumental developments are concerned, it seems that at least four tracks can be foreseen for future research.

In the first place, there seems to be no reason why additional unstable species and molecular complexes would not be observed and studied using FT–jet facilities. Such developments are most probably only available for those groups having developed set-ups achieving very cold translational temperatures, thus using single pinholes and multi-pass optics. In any such event, however, the studies will have to cope with the limited spectral resolution, also reducing the signal-to-noise ratio, when using FTS. However, many developments along this research direction can certainly be accomplished before irremediably facing this limitation.

In the second place, more detailed studies of vibrational temperatures, and of

energy transfers than those so far published seem readily achievable. Compared with tunable laser-based investigations, FT–jet spectroscopy allows wider spectral ranges to be probed, giving an easier access to relevant data in this context. Relative intensity measurements are however concerned with this type of investigation, whose precision is still to be somewhat assessed in FT–jet experiments.

In the third place, one could expect larger organic species to become favourite targets of future investigation, thus extending the initial contribution by Snavely concerning benzene [89]. It is likely that the problem to be faced, also encountered in laser investigations, is the clustering of the species in the jet, whose efficiency might be directly related to the vapour pressure of the sample. Most of the larger organic species are indeed liquid under STP conditions. The experimental conditions required with FT–jets to achieve similar signal-to-noise ratios as with lasers, unfortunately call for significantly larger amounts of sample, thus probably raising the clustering effects during the formation of the supersonic jet stream. This problem was tentatively faced at ULB using a pulsed inlet of material in a heated volume, prior to the injection in the slit. Such a set-up was tested with success with methanol [44]. Other liquid species under STP conditions were investigated with, however, so far limited results, probably because of the weakness of the infrared absorption bands in larger species, relative to the smaller ones, which strongly limit the signal-to-noise ratio.

It should be mentioned that the cluster formation just mentioned opens up, on the other hand, a research field ideally suited for FT spectroscopy studies. Indeed, large spectral ranges can be covered and only medium resolution is required given the lack of rotational structure in larger clusters. In addition, FTS are capable of investigating quasi continuum absorption features, which is not the case with several laser based techniques. This trend for future investigations is certainly emerging from recent studies [22, 160, 161] and might prove to be a central issue for FT–jet spectroscopy. This field is of high interest but, however, does not fit the field of *high resolution* spectroscopy anymore.

In the final place, higher sensitivity could be reached using improved designs based on longer slits and multi-pass absorption possibly achieved within a laser cavity. Such developments would lead to advances in a number of fields, including overtone spectroscopy of larger species at chemically significant energy.

Acknowledgements

We are grateful to a number of colleagues and friends for their help: Mr P. Joubert for the picture of the multinozzle expansion; Dr Demaison (PhLAM, Lille I), for providing useful references; various authors of the referenced works, for providing preprints and original of figures; all collaborators who participated in the ULB work involved in this review, in particular Professors/Drs Durry (Service d'Aéronomie, Verrières-le-Buisson), Holland (Industry) and Mélen (ULg, Belgium), Coudert, Flaud, Kleiner, Perrin (PPM, Orsay), Boudon, Hilico, Pierre (LP, Dijon), Jost (LCMI, Grenoble), Lafferty (NIST, Washington) and, from CPM-ULB, Drs Carleer, Liévin and Vander Auwera, Mr Bach, Mr Herregodts and Mr Mellouki and, with special thanks, the technical staff composed of Mr Pétrisse, Mrs Rizopoulos and Mr Walgraeve; Dr Demaison (ULille1), Dr Campargue (U. J. Fourier) and Professor Sutcliffe (ULB), for reading the manuscript; and FNRS, EC and ULB who provided financial support for the ULB work involved in this review.

References

[1] Smalley, R. E., Wharton, L., and Levy, D. H., 1975, *J. chem. Phys.*, **63**, 4977.
[2] Levy, D. H., 1980, *Ann. Rev. phys. Chem.*, **31**, 197.
[3] Leopold, K. R., Fraser, G. T., Novick, S. E., and Klemperer, W., 1994, *Chem. Rev.*, **94**, 1807.
[4] Bettens, F. L., Bettens, R. P. A., and Bauder, A., 1995, *Jet Spectroscopy and Molecular Dynamics*, edited by J. M. Hollas and D. Phillips (Edinburgh: Blackie), Chap. I, p. 1.
[5] Huber, K. P., and Sears, T. J., 1985, *Chem. Phys. Lett.*, **113**, 129.
[6] Huber, K. P., 1986, *J. molec. Spectrosc.*, **119**, 433.
[7] Haridass, C., and Huber, K. P., 1994, *Astrophys. J.*, **420**, 433.
[8] Ito, K., Huber, K. P., Yoshino, K., Ogawa, M., and Morioka, Y., 1995, *J. molec. Spectrosc.*, **171**, 1.
[9] Snavely, D. L., Colson, S. D., and Wiberg, K. B., 1981, *J. chem. Phys.*, **74**, 6975.
[10] Scherer, J. J., Paul, J. B., O Keefe, A., and Saykally, R. J., 1997, *Chem. Rev.*, **97**, 25.
[11] Herman, M., Liévin, J., Vander Auwera, J., and Campargue, A., 1999, *Adv. chem. Phys.*, **108**, 1.
[12] Winnewisser, G., Drascher, T., Giesen, T., Pak, I., Schmülling, F., and Schieder, R., 1999, *Spectrochim. Acta*, **A55**, 2121.
[13] Dübal, H.-R., Quack, M., and Schmitt, U., 1984, *Chimia*, **38**, 438.
[14] Barnes, J. A., and Gough, T. E., 1987, *J. chem. Phys.*, **86**, 6012.
[15] Walters, A. D., Winnewisser, M., Lattner, K., and Winnewisser, B. P., 1991, *J. molec. Spectrosc.*, **149**, 542.
[16] Holland, J. K., Carleer, M., Pétrisse, R., and Herman, M., 1992, *Chem. Phys. Lett.*, **194**, 175.
[17] Meads, R. F., Hartz, C. L., Lucchese, R. R., and Bevan, J. W., 1993, *Chem. Phys. Lett.*, **206**, 488.
[18] McNaughton, D., McGilvery, D., and Robertson, E. G., 1994, *J. chem. Soc. Faraday Trans.*, **90**, 1055.
[19] Asselin, P., Soulard, P., Tarrago, G., Lacome, N., and Manceron, L., 1996, *J. chem. Phys.*, **104**, 4427.
[20] Benidar, A., Georges, R., Le Doucen, R., Boissoles, J., Hamon, S., Canosa, A., and Rowe, B. R., 1999, *J. molec. Spectrosc.*, **199**, 92.
[21] Häber, T., Schaal, H., Schmitt, U., and Suhm, M. A., 1999, *XVI International Conference on Molecular Energy Transfer*, June 1999, Assisi, Italy, abstract 79-TU.
[22] Häber, T., Schmitt, U., and Suhm, M. A., 1999, *Phys. Chem. Chem. Phys.*, **1**, 5573.
[23] Guelachvili, G., and Picqué, N., 1999, private communication; Picqué, N., 1998, PhD thesis, Université Paris Sud, France.
[24] Mélen, F., Pokorni, F., and Herman, M., 1992, *Chem. Phys. Lett.*, **194**, 181.
[25] Herman, M., 1992, unpublished results,
[26] Hepp, M., Georges, R., Herman, M., Flaud, J.-M., and Lafferty, W. J., 2000, *J. molec. Struct.*, **517**, 171.
[27] Mélen, F., Carleer, M., and Herman, M., 1992, *Chem. Phys. Lett.*, **199**, 124.
[28] Luckhaus, D., and Quack, M., 1992, *Chem. Phys. Lett.*, **199**, 293.
[29] Luckhaus, D., and Quack, M., 1993, *J. molec. Struct.*, **293**, 213.
[30] Domenech, J. L., Andrews, A. M., Belov, S. P., Fraser, G. T., and Lafferty, W. J., 1994, *J. chem. Phys.*, **100**, 6993.
[31] Michelson, A. A., 1895, *Astrophys. J.*, **2**, 251.
[32] Bell, R. J., 1972, *Introductory Fourier Transform Spectroscopy* (New York, London: Academic Press), p. 382.
[33] Griffiths, P. R., and de Haseth, J. A., 1986, *Fourier Transform Infrared Spectrometry* (New York: Wiley).
[34] Connes, J., 1961, *Rev. Opt. theor. instrum.*, **40**, 45.
[35] Connes, J., 1961, *Rev. Opt. theor. instrum.*, **40**, 116.
[36] Connes, J., 1961, *Rev. Opt. theor. instrum.*, **40**, 171.
[37] Connes, J., 1961, *Rev. Opt. theor. instrum.*, **40**, 231.
[38] Connes, J., Delouis, H., Connes, P., Guelachvili, G., Maillard, J.-P., and Michel, G., 1970, *Nouv. Rev. Opt. appl.*, **1**, 3.
[39] Connes, P., 1970, *Ann. Rev. Astron. Astrophys.*, **8**, 209.

[40] Connes, P., and Michel, G., 1975, *Appl. Optics*, **4**, 2067.
[41] Guelachvili, G., 1978, *Appl. Opt.*, **17**, 1322.
[42] Cooley, J. W., and Tuckey, J. W., 1965, *Math. Comput.*, **19**, 297.
[43] Brigham, E. O., 1974, *The Fast Fourier Transform* (Englewood Cliffs, NJ: Prentice-Hall), p. 252.
[44] Hepp, M., Herregodts, F., and Herman, M., 1998, *Chem. Phys. Lett.*, **294**, 528.
[45] Bevan, J. W., 1994, *Faraday Discuss.*, **97**, 180.
[46] Scherer, J. J., Voelkel, D., Rakestraw, D. J., Paul, J. B., Collier, C. P., Saykally, R. J., and O'keefe, A., 1995, *Chem. Phys. Lett.*, **245**, 273.
[47] Scherer, J. J., Paul, J. B., O'keefe, A., and Saykally, R. J., 1997, *Chem. Rev.*, **97**, 25.
[48] Hagena, O. F., 1981, *Surf. Sci.*, **106**, 101.
[49] Campargue, R., 1984, *J. phys. Chem.*, **88**, 4466.
[50] McKellar, A. R. W., 1988, *J. chem. Phys.*, **88**, 4190.
[51] Messer, J. K., and De Lucia, F. C., 1984, *Phys. Rev. Lett.*, **53**, 2555.
[52] DePaul, S., Pullman, D., and Friedrich, B., 1993, *J. phys. Chem.*, **97**, 2167.
[53] Miller, D. R., 1988, *Atomic and Molecular Beam Methods*, Vol. I, edited by G. Scoles (Oxford: Oxford University Press), Chap. 2, p. 14.
[54] Lovejoy, G., 1991, PhD thesis, *JILA*, Boulder.
[55] Liepmann, H. W., and Roshko, A., 1957, *Elements of Gas Dynamics* (New York: Wiley), Chap. 2.
[56] Sulkes, M., Jouvet, C., and Rice, S. A., 1982, *Chem. Phys. Lett.*, **87**, 515.
[57] Amrein, A., Quack, M., and Schmitt, U., 1987, *Z. phys. Chem.*, **154**, 59.
[58] Amrein, A., Hollenstein, H., Locher, P., Quack, M., Schmitt, U., and Bürger, H., 1987, *Chem. Phys. Lett.*, **139**, 82.
[59] Amrein, A., Quack, M., and Schmitt, U., 1988, *J. phys. Chem.*, **92**, 5455.
[60] Schaefer, M., and Bauder, A., 1999, *Chem. Phys. Lett.*, **308**, 355.
[61] Petry, R., Klee, S., Lock, M., Winnewisser, B. P., and Winnewisser, M., 1999, private communication,
[62] El Youssoufi, Y., Georges, R., Liévin, J., and Herman, M., 1997, *J. molec. Spectrosc.*, **186**, 239.
[63] Hepp, M., Winewisser, G., and Yamada, K. M. T., 1994, *J. molec. Spectrosc.*, **164**, 311.
[64] Georges, R., Herman, M., Hillico, J. C., and Robert, D., 1998, *J. molec. Spectrosc.*, **187**, 13.
[65] Boraas, K., Lin, Z., and Reilly, J. P., 1994, *J. chem. Phys.*, **100**, 7916.
[66] Campargue, A., Permogorov, D., and Jost, R., 1995, *J. chem. Phys.*, **102**, 5910.
[67] Luckhaus, D., Quack, M., Schmitt, U., and Suhm, M. A., 1995, *Ber. Bunsenges. phys. Chem.*, **99**, 457.
[68] Suhm, M. A., 1995, *Ber. Bunsenges. phys. Chem.*, **99**, 1159.
[69] Quack, M., Schmitt, U., and Suhm, M. A., 1997, *Chem. Phys. Lett.*, **269**, 29.
[70] Engeln, R., and Meier, G., 1996, *Rev. sci. Instrum.*, **67**, 2708.
[71] Durry, G., 1994, PhD thesis, Université de Paris-Sud, Orsay, France, p. 149.
[72] Durry, G., and Guelachvili, G., 1994, *J. molec. Spectrosc.*, **168**, 82.
[73] Durry, G., and Guelachvili, G., 1995, *Vib. Spectrosc.*, **8**, 255.
[74] Durry, G., and Guelachvili, G., 1995, *Appl. Optics*, **34**, 1971.
[75] Durry, G., and Guelachvili, G., 1995, *J. opt. Soc. Am.* B, **12**, 1555.
[76] Picqué, N., and Guelachvili, G., 2000, *Appl. Optics*, in the press.
[77] Fletcher, T. R., and Leone, S. R., 1988, *J. chem. Phys.*, **88**, 4720.
[78] Rogers, S. A., and Leone, S. R., 1993, *Appl. Spectrosc.*, **47**, 1430.
[79] Lindner, J., Stahlhut, O., Wilhelm, R., and Ermisch, K., 1998, *Rev. sci. Instrum.*, **69**, 1629.
[80] Hu, S., Lin, H., He, S., Cheng, J., and Zhu, Q., 1999, *Phys. Chem. Chem. Phys.*, **1**, 3727.
[81] Cheng, J.-X., Lin, H., Hu, S.-G., He, S.-G., Zhu, Q.-S., and Kachanov, A. A., 2000, *J. chem. Phys.* (to be published).
[82] Ashkenas, H., and Sherman, F. S., 1966, The structure and utilization of supersonic free jets in low density wind tunnels in *Rarefied Gas Dynamics, 4th Symposium*, edited by J. H. Leeuw *et al.* (New York: Academic Press).
[83] Ballard, J., Newnham, D., and Page, M., 1993, *Chem. Phys. Lett.*, **208**, 295.
[84] Snavely, D. L., Wiberg, K. B., and Colson, S. D., 1983, *Chem. Phys. Lett.*, **96**, 319.

[85] McNaughton, D., Evans, C., and Robertson, E. G., 1995, *J. chem. Soc. Faraday Trans. 2*, **91**, 1723.
[86] McNaughton, D., McGilvery, D., and Robertson, E. G., 1995, *J. molec. Struct.*, **348**, 1.
[87] McNaughton, D., Evans, C., and Robertson, E. G., 1996, *Mikrochim. Acta*, **14**, 543.
[88] McNaughton, D., Robertson, E. G., and Shanks, F., 1996, *Chem. Phys.*, **206**, 161.
[89] Snavely, D. L., Walters, V. A., Colson, S. D., and Wiberg, K. B., 1984, *Chem. Phys. Lett.*, **103**, 423.
[90] Walters, V. A., Snavely, D. L., Colson, S. D., Wiberg, K. B., and Wong, K. N., 1986, *J. phys. Chem.*, **90**, 592.
[91] Amrein, A., Dübal, H. R., and Quack, M., 1985, *Molec. Phys.*, **56**, 727.
[92] Amrein, A., Quack, M., and Schmitt, U., 1987, *Molec. Phys.*, **60**, 237.
[93] Bürger, H., Rahner, A., Amrein, A., Hollenstein, H., and Quack, M., 1989, *Chem. Phys. Lett.*, **156**, 557.
[94] Bürger, H., Goergens, U., Ruland, H., Quack, M., and Schmitt, U., 1996, *Molec. Phys.*, **87**, 469.
[95] Hollenstein, H., Quack, M., and Richard, E., 1994, *Chem. Phys. Lett.*, **222**, 176.
[96] Quack, M., Schmitt, U., and Suhm, M. A., 1993, *Chem. Phys. Lett.*, **208**, 446.
[97] Ross, A. J., Amrein, A., Luckhaus, D., and Quack, M., 1989, *Molec. Phys.*, **66**, 1273.
[98] Snels, M., and Quack, M., 1991, *J. chem. Phys.*, **95**, 6355.
[99] Snels, M., Beil, A., Hollenstein, H., Quack, M., Schmitt, U., and D'Amato, F., 1995, *J. chem. Phys.*, **103**, 8846.
[100] Asselin, P., Dupuis, B., Perchard, J. P., and Soulard, P., 1997, *Chem. Phys. Lett.*, **268**, 265.
[101] Asselin, P., Soulard, P., and Lacome, N., 1998, *J. molec. Spectrosc.*, **190**, 274.
[102] Bach, M., Georges, R., Hepp, M., and Herman, M., 1998, *Chem. Phys. Lett.*, **294**, 533.
[103] Bach, M., Georges, R., Herman, M., and Perrin, A., 1999, *Molec. Phys.*, **97**, 265.
[104] Boudon, V., Hepp, M., Herman, M., Pak, I., and Pierre, G., 1998, *J. molec. Spectrosc.*, **192**, 359.
[105] Georges, R., Durry, G., Bach, M., Pétrisse, R., Jost, R., and Herman, M., 1995, *Chem. Phys. Lett.*, **246**, 601.
[106] Georges, R., Liévin, J., Herman, M., and Perrin, A., 1996, *Chem. Phys. Lett.*, **256**, 675.
[107] Georges, R., Bach, M., and Herman, M., 1997, *Molec. Phys.*, **90**, 381.
[108] Hepp, M., Georges, R., and Herman, M., 1997, *Chem. Phys. Lett.*, **275**, 513.
[109] Hepp, M., and Herman, M., 1998, *Molec. Phys.*, **94**, 829.
[110] Kleiner, I., Georges, R., Hepp, M., and Herman, M., 1999, *J. molec. Spectrosc.*, **193**, 228.
[111] Barnes, J. A., and Gough, T. E., 1986, *Chem. Phys. Lett.*, **130**, 297.
[112] Barnes, J. A., Douketis, C., Gibson, J. G., and Gough, T. E., 1992, *Chem. Phys. Lett.*, **200**, 274.
[113] Han, J., Wang, Z., McIntosh, A. L., Lucchese, R. R., and Bevan, J. W., 1994, *J. chem. Phys.*, **100**, 7101.
[114] Hartz, C. L., Wofford, B. A., McIntosh, A. L., Meads, R. F., Lucchese, R. R., and Bevan, J. W., 1995, *Ber. Bunsenges. phys. Chem.*, **99**, 447.
[115] Meads, R. F., McIntosh, A. L., Arno, J. I., Hartz, C. L., Lucchese, R. R., and Bevan, J. W., 1994, *J. chem. Phys.*, **101**, 4593.
[116] Brazier, C. R., Carrick, P. G., and Bernath, P. F., 1992, *J. chem. Phys.*, **96**, 919.
[117] O'Brien, L. C., Brazier, C. R., and Bernath, P. F., 1987, *J. molec. Spectrosc.*, **124**, 489.
[118] Oliphant, N., Lee, A., and Bernath, P. F., 1990, *J. chem. Phys.*, **1990**, 2244.
[119] Prasad, C. V. V., Bernath, P. F., Frum, C., and Engleman Jr, R., 1992, *J. molec. Spectrosc.*, **151**, 459.
[120] Prasad, C. V. V., and Bernath, P. F., 1992, *J. molec. Spectrosc.*, **156**, 327.
[121] Prasad, C. V. V., and Bernath, P. F., 1994, *Astrophys. J.*, **426**, 812.
[122] Davies, P. B., Martin, N. A., Nunes, M. D., Pape, D. A., and Russell, D. K., 1990, *J. chem. Phys.*, **93**, 1576.
[123] Frost, G. J., Goss, L. M., and Vaida, V., 1996, *J. geophys. Res.*, **101**, 3869.
[124] Richard, E. C., Donaldson, D. J., and Vaida, V., 1989, *Chem. Phys. Lett.*, **157**, 295.
[125] Richard, E. C., and Vaida, V., 1991, *J. chem. Phys.*, **94**, 163.

[126] RICHARD, E. C., and VAIDA, V., 1991, *J. chem. Phys.*, **94**, 153.
[127] GAUTHIER, M., 1988, *J. chem. Phys.*, **88**, 5439.
[128] REHFUSS, B., SUH, M., MILLER, T. A., and BONDYBEY, V., 1992, *J. molec. Spectrosc.*, **151**, 437.
[129] GROSS, M., HERMANN, G., and SCHARMANN, A., 1989, *Spectrochim. Acta*, **44B**, 597.
[130] JOST, R., 1995, private communication.
[131] KULEZNEV, E. V., BARANOV, V. I., and TRUBNIKOV, D. N., 1994, *Chem. Phys. Lett.*, **223**, 255.
[132] GEORGES, R., and HERMAN, M., 1995, unpublished results,
[133] JOST, R., 1994, private communication.
[134] ARNO, J., and BEVAN, J. W., 1995, *Jet Spectroscopy and Molecular Dynamics*, edited by J. M. Hollas and D. Phillips (Edinburgh: Blackie), p. 29.
[135] DUPEYRAT, G., 1980, *Progress in Astronautics and Aeronautics*, edited by S. S. Fisher (New York: AIAA), p. 812.
[136] RYALI, S. B., and FENN, J. B., 1984, *Ber. Bunsenges. phys. Chem.*, **88**, 245.
[137] MURPHY, H. R., and MILLER, D. R., 1984, *J. phys. Chem.*, **88**, 4474.
[138] ABRAHAM, O., KIM, S. S., and STEIN, G. D., 1981, *J. chem. Phys.*, **75**, 402.
[139] TANIMURA, S., OKADA, Y., and TAKEUCHI, K., 1996, *J. phys. Chem.*, **100**, 2842.
[140] DUPEYRAT, G., MARQUETTE, J. B., and ROWE, B. R., 1985, *Phys. Fluids*, **28**, 121.
[141] SLOAN, J. J., and KRUUS, E. J., 1989, *Time Resolved Spectroscopy*, edited by R. J. H. Clarck and R. E. Hester (New York: Wiley).
[142] MÉLEN, F., HERMAN, M., MATTI, G. Y., and MCNAUGHTON, D. M., 1993, *J. molec. Spectrosc.*, **160**, 601.
[143] NAKANAGA, T., ITO, F., and TAKEO, H., 1993, *Bull. Inst. Chem. Res.*, Kyoto Univ., **71**, 140.
[144] KLEE, S., and OGILVIE, J. F., 1993, *Spectrochim. Acta*, **49A**, 345.
[145] AMREIN, A., HOLLENSTEIN, H., QUACK, M., and SCHMITT, U., 1989, *Infrared Phys.*, **29**, 561.
[146] AMREIN, A., LUCKHAUS, D., MERKT, F., and QUACK, M., 1988, *Chem. Phys. Lett.*, **152**, 275.
[147] HERMAN, M., HERREGODTS, F., GEORGES, R., HEPP, M., HADJ BACHIR, I., LECOUTRE, M., and KLEINER, I., 1999, *Chem. Phys.*, **246**, 433.
[148] HEPP, M., and HERMAN, M., 1999, *J. molec. Spectrosc.*, **194**, 87.
[149] HEPP, M., and HERMAN, M., 1999, *J. molec. Spectrosc.*, **197**, 56.
[150] MCNAUGHTON, D., and EVANS, C., 1996, *J. phys. Chem.*, **100**, 8660.
[151] MCNAUGHTON, D., and EVANS, C., 1997, *J. molec. Spectrosc.*, **182**, 342.
[152] KLEINER, I., FLAUD, J.-M., LAFFERTY, W., RIZOPOULOS, A., and HERMAN, M., 2000, in preparation,
[153] CARCABAL, P., CHEVALIER, M., BROQUIER, M., COUDERT, L. H., HEPP, M., and HERMAN, M., 1999, *16th Colloquium on High Resolution Molecular Spectroscopy*, Université de Bourgogne, Abstract L25.
[154] MELLOUKI, A., GEORGES, R., HERMAN, M., SNAVELY, D. L., and LEYTNER, S., 1997, *Chem. Phys.*, **220**, 311.
[155] MCNAUGHTON, D., and EVANS, C. J., 1999, *Spectrochim. Acta*, **A55**, 1177.
[156] LESPADE, L., CAVAGNAT, D., RODIN-BERCION, S., and MANCERON, L., 1999, *16th Colloquium on High Resolution Molecular Spectroscopy*, Dijon, Université de Bourgogne, Abstract M26.
[157] BOUDON, V., ROTGER, M., HE, Y., HOLLENSTEIN, H., QUACK, M., and SCHMITT, U., 1999, *16th Colloquium on High Resolution Molecular Spectroscopy*, Dijon, Université de Bourgogne, Abstract F9.
[158] ASSELIN, P., SOULARD, P., MANCERON, L., BOUDON, V., and PIERRE, G., 2000, *J. molec. Struct.*, **517**, 145.
[159] QUACK, M., and SUHM, M. A., 1998, *Adv. molec. Vib. collision Dyn.*, **3**, 205.
[160] ASSELIN, P., SOULARD, P., and PERCHARD, J. P., 1999, *Chem. Phys.*, **249**, 73.
[161] SCHAAL, H., HÄBER, T., and SUHM, M. A., 2000, *J. phys. Chem.* A, **104**, 265.
[162] RICHARD, E. C., WICKHAM-JONES, C. T., and VAIDA, V., 1989, *J. phys. Chem.*, **93**, 6346.
[163] LINDNER, J., ERMISCH, K., and WILHELM, R., 1998, *Chem. Phys.*, **238**, 329.
[164] HUBER, K.-P., and VERVLOET, M., 1988, *J. chem. Phys.*, **89**, 5957.
[165] HUBER, K.-P., and VERVLOET, M., 1992, *J. molec. Spectrosc.*, **153**, 17.

[166] ROUX, F., MICHAUD, F., and VERVLOET, M., 1994, *J. molec. Spectrosc.*, **164**, 510.
[167] HUBER, K.-P., VERVLOET, M., JUNGEN, C., and ROCHE, A. L., 1987, *Molec. Phys.*, **61**, 501.
[168] HUBER, K.-P., and VERVLOET, M., 1988, *J. molec. Spectrosc.*, **129**, 1.
[169] ANDERSON, B. D., YU, T., MCKEOWN, P. J., and JOHNSTON, M. V., 1988, *Appl. Spectrosc.*, **42**, 1121.
[170] ROSS, A. J., CROZET, P., BACIS, R., CHURASSY, S., ERBA, B., ASHWORTH, S. H., LAKIN, N. M., WICKHAM, M. R., BEATTIE, I. R., and BROWN, J. M., 1996, *J. molec. Spectrosc.*, **177**, 134.
[171] CARRICK, P. G., BRAZIER, C. R., BERNATH, P. F., and ENGELKING, P. C., 1987, *J. Am. chem. Soc.*, **109**, 5100.
[172] SUH, M. H., LEE, S. K., and MILLER, T. A., 1999, *J. molec. Spectrosc.*, **194**, 211.
[173] SUH, M. H., LEE, S. K., REHFUSS, B. D., MILLER, T. A., and BONDYBEY, V. E., 1991, *J. phys. Chem.*, **95**, 2727.
[174] MANTELL, D. A., RYALI, S. B., HALPERN, B. L., HALLER, G. L., and FENN, J. B., 1981, *Chem. Phys. Lett.*, **81**, 185.
[175] MANTELL, D. A., RYALI, S. B., HALLER, G. L., and FENN, J. B., 1983, *J. chem. Phys.*, **78**, 4250.
[176] VENKATESHAN, S. P., RYALI, S. B., and FENN, J. B., 1982, *J. chem. Phys.*, **77**, 2599.
[177] LINDNER, J., LOOMIS, R. A., KLAASEN, J. J., and LEONE, S. R., 1998, *J. chem. Phys.*, **108**, 1944.
[178] FENN, J. B., 1996, *Ann. Rev. phys. Chem.*, **47**, 1.
[179] QUACK, M., 1990, *Ann. Rev. phys. Chem.*, **41**, 839.
[180] SLOAN, J. J., 1992, *Atomic and Molecular Beam Methods*, Vol. II, edited by G. Scoles (New York: Oxford University Press), Chap. 10.
[181] GEORGES, R., BACH, M., and HERMAN, M., 1999, *Molec. Phys.*, **97**, 279.
[182] OOMENS, J., OUDEJANS, L., REUSS, J., and FAYT, A., 1994, *Chem. Phys.*, **187**, 57.
[183] OOMENS, J., REUSS, J., MELLAU, G. C., KLEE, S., GULACZYK, I., and FAYT, A., 1996, *J. molec. Spectrosc.*, **180**, 236.
[184] HENRY, L., VALENTIN, A., LAFFERTY, W. J., HOUGEN, J. T., DEVI, V. M., DAS, P. P., and RAO, K. N., 1983, *J. molec. Spectrosc.*, **100**, 260.
[185] HEPP, M., and HERMAN, M., 2000, *Molec. Phys.*, **98**, 57.
[186] MÉLEN, F., and HERMAN, M., 1992, *J. phys. Chem. Ref. Data*, **21**, 831.
[187] SCHERER, M., and HAVENITH, M., 1997, *Colloquium on High Resolution Molecular Spectroscopy*, Glasgow, edited by G. Duxburry, abstract K2.
[188] WATSON, J. K. G., and MCKELLAR, A. R. W., 1997, *Can. J. Phys.*, **75**, 181.